Title
Distinct plasmablast developmental intermediates produce graded expression of IgM secretory transcripts

Journal
Cell Reports, 44(2)

ISSN
2639-1856

Authors
Sievert, Evelyn P
Franke, Marissa C
Thomas, Kayla B
et al.

Publication Date
2025-02-01

DOI
10.1016/j.celrep.2025.115283

Distinct Plasmablast developmental intermediates produce graded expression of IgM secretory transcripts

Evelyn P. Sievert[1], Marissa C. Franke[1], Kayla B. Thomas[1], Yoseop Yoon[2], Yongsheng Shi[2,*], Roger Sciammas[1,3*]

[1]Department of Anatomy, Physiology, and Cell Biology, University of California at Davis; Davis, CA USA

[2]Department of Microbiology and Molecular Genetics, School of Medicine, University of California at Irvine; Irvine, CA USA

[3]Lead contact

*Correspondence to YS (yongshes@uci.edu) & RS (rsciammas@ucdavis.edu)

Summary

Differentiation into plasma cells (PC) enables secretion of ~10,000 immunoglobulin molecules per second. This extraordinary capacity requires the upregulation of PC transcriptional determinants that specify PC fate, increase immunoglobulin mRNA synthesis, coordinate alternative 3'end processing of the heavy chain transcript from the distal to proximal poly-adenylation site (PAS), and remodel the secretory pathway. We developed a dual-fluorescent protein reporter mouse to prospectively study the post-transcriptional-level transition from membrane-anchored to secretory immunoglobulin M; µM-PAS and µS-PAS, respectively. We observed (i) graded µS-PAS usage during PC differentiation (ii) IRF4 and Blimp-1 functioned hierarchically to increase µ abundance as well as µS-PAS usage and (iii) graded µS populations did or did not express Blimp-1. Interestingly, the low and high µS and Blimp-1-expressing populations arose from distinct developmental intermediates that exhibited dissimilar endoplasmic reticulum features. The distinct cell and µS-PAS fate trajectories may have implications for derivatization of the secretory pathway.

Introduction

The rearranged antigen receptor genes are integral to the B and T cell lineages; however, in contrast to T cells, B cells have evolved elaborate systems of modifying their receptor genes to enable distinct effector functions during productive immune responses. Specifically, targeted somatic hypermutation (SHM) of germline Immunoglobulin (Ig) heavy chain VDJ and light chain VJ segments, class switch recombination (CSR) to exchange germline μ constant regions for γ, α, and ε variants, as well as post-transcriptional regulation of the Ig heavy (IgH) chain primary transcript that promotes usage of a distinct 3' end encoding a COOH-modified gene product that is secreted rather than membrane-anchored[1]. These processes are deployed in specialized B cells: Germinal Center B cells (GCBs) undergo SHM and CSR, activated B cells undergo CSR, and plasma cells (PCs) engage alternative 3' end processing[2]. All processes have been extensively studied; however, despite the ~40-year knowledge of alternative 3' end processing of the IgH pre-mRNA[3–5], significant elements of the process remain speculative.

Groundbreaking research using lymphoma and myeloma cell lines demonstrated that alternative 3' end processing targeting the μS poly-adenylation site (PAS) of the IgH transcript is a specialized property of PCs[6]. Note that the exonic and PAS architecture is common to all constant region isotypes implying a conserved mechanism. Sequential activation of the IRF4 and Blimp-1 transcription factors directs PC differentiation and analysis of loss of function mutations of each demonstrate that they are essential for both PC fate and secretory capacity[7,8]. Conversely, ectopic expression of each in B cells promotes PC differentiation. IRF4 expression is induced by BCR, CD40, and TLR signaling which in turn functions to activate expression of the Blimp-1 transcription factor as well as promote the survival of PCs[9,10]. Blimp-1 cements the PC fate by repressing the expression of the B lineage promoting transcription factor genes cRel, Bcl6, Bach2,

Ebf1, and Pax5, which themselves antagonize the expression of IRF4 and/or Blimp-1 as well as components of the PC gene program[11]. IRF4 and Blimp-1 also elaborate a PC gene program, in part based on enhancing Xbp-1s activity, that is focused on the secretory pathway to promote high-rate antibody synthesis and secretion which can reach upwards of thousands of molecules per second[12]. Analysis of Irf4 or Blimp-1 mutant B cells and animals demonstrate marked reduction in alternative 3' end processing of the IgH transcript and consequently display considerably diminished serum Ig. Of note, conditional Blimp-1 mutant animals accumulate low amounts of serum Ig compared to Rag mutants (which are devoid of rearranged antibody genes and B cells). The discrepancy is thought to be attributable to (i) differentiation of Blimp-1 independent pre-PCs that secrete at low levels[13], (ii) Blimp-1-independent B1 secreting cells[14], and/or (iii) stochastic usage of the μS PAS. Support for the last possibility comes from the observation that germline transcripts produced in proB cells are processed using the μS PAS at some frequency[15]. Overall, although Blimp-1 strongly promotes alternative 3' end processing of IgH, it may not be an absolute requirement.

The default cleavage and polyadenylation (CPA) event on the distal μM PAS occurs at all stages of B cell development and activation but infrequently in PCs[16]. The default choice is due to a splicing event that removes the proximal μS PAS, F1A. In contrast, in PCs, such splicing is suppressed in favor of CPA at the proximal μS PAS. Pioneering work by Peterson and Milcarek has shown that CPA, but not splicing, is the post-transcriptional determinant regulated in PCs[17,18]. Also, it has been demonstrated that transcriptional upregulation by IRF4 and Blimp-1[19–21] of the RNA polymerase II (RPA2) elongation factor, ELL2, during PC differentiation promotes CPA at the μS PAS[19]. It is noteworthy that during PC differentiation, activated B cells greatly increase synthesis of IgH transcripts[22] supporting a model where increased synthesis and preferential

proximal CPA are coordinated[23]. Importantly, variable spot sizes in ELISpot experiments demonstrate that secretory capacity is heterogenous but the basis of which is only beginning to be explored[24,25]. Together, basic questions about the temporal regulation of IgH transcript synthesis and PAS usage remain unanswered, principally because of the absence of a single-cell perspective of these events during PC differentiation.

Tracking μS PAS usage during the transition to PC differentiation is limited to ELISA/ELISpot, population-based RNA detection methods, or the acquisition of PC markers warranting an emergent approach to better understand the dynamics of alternate 3' end processing of the IgH transcript. This lack of precision motivated us to construct a model to prospectively identify such cells. Herein, we analyze a dual reporter mouse that we engineered to express fluorescent proteins based on μS or μM PAS usage. Our analysis demonstrates (i) graded expression of μS PAS usage that is dependent on IRF4 and Blimp-1 (ii) an IRF4 dependent, yet Blimp-1 independent increase in μ synthesis and as well as a Blimp-1-dependent increase in μS PAS usage (iii) the existence of a population of cells that exhibit high rates of μS PAS usage that do not express Blimp-1 and (iv) a distinct cell fate branch point in deployment of graded μS PAS usage. The combined single cell analysis reveals a greater complexity to PC differentiation and μS PAS usage than previously predicted.

Results

Development of μReporter mice. A prospective approach to identify cells at the onset and/or during μS PAS usage of the IgH transcript would enable timely isolation of such cells for analysis as well as to correlate with attributes of PC fate. Although it would be advantageous to tag the PAS of all constant region isotypes, their duplication and physical separation makes it technically

challenging. The proximal and distal PAS of the µ IgH locus are separated by ~1.5kb of DNA enabling assembly of a single targeting construct composed of spectrally distinct fluorescent protein ORFs to be placed upstream of both the µS and µM PAS, **F1B (**see STAR methods). Heterozygous µReporter (µR) mice were used throughout our experiments and were compared to wild type non-fluorescent littermates.

Analysis of µReporter B cells. µReporter mice produced B cells of comparable percentages and numbers as wild type counterparts, **SF2A**. Based on pioneering work with murine lymphomas and plasmacytomas, we reasoned that non-PC µ-expressing B cells would predominantly express high levels of µM:mKO2 accompanied with little to no µS:mA fluorescence. Furthermore, we predicted that rare PC µ-expressing B cells would be low/absent for µM:mKO2 fluorescence and bright for µS:mA. In contrast to our expectations, analysis of µR splenic B cells at steady state demonstrated coexpression of µM:mKO2 and µS:mA by many B220+ B cells, **F1C**. A minority of the B220+ cells predominantly expressed µS:mA only; this observation as well as those in **F3A,C and F5B** suggests that the mA fluorescence does not overlap that of mKO2. A population of non-fluorescent B220+ B cells is also apparent (compare to C57Bl/6 control) and predicted by virtue of intact allelic exclusion and/or CSR[26]. In addition, moderate fluorescence was observed in T cells which is predicted based on precocious µ germline transcript expression (GLT) in T cells[27]. The expression of µM:mKO2 fluorescence was reliable as the cells were efficiently stained with anti-IgM antibodies, **F1D**.

Published results that enumerated rare µ-secreting cells by ELISpot from spleen suggests that the µS:mA fluorescence pattern at this population-level resolution is confounding[14]. We reasoned that this outcome could be attributed to expression of µ GLT and/or a given rate of stochastic µS PAS usage. For the former, such a mechanism would not be unprecedented as previous work has

demonstrated efficient translation of μ GLT[28]. In support of this latter notion, rare switched (thus deleted for the μ locus) IgG1 B cells ex vivo displayed no μS:mA or μM:mKO2 reporter expression, **F1E**. Thus, while the mA-H2B fusion protein may be highly durable, this observation also suggests ongoing translation maintains its expression. Furthermore, GCBs display greatly diminished μS:mA expression (**F1F**), consistent with their non-secretory phenotype as well as their high rates of proliferation and catabolic activity, which would dilute and degrade μS:mA protein, respectively. In contrast, a fraction of GCBs appropriately expressed μM:mKO2. Interestingly, GCBs displayed a higher frequency of non-fluorescent cells, consistent with the high rates of CSR, resulting in deletion of the μ locus[29]. Thus, under specific circumstances, the patterns of μS:mA and μM:mKO2 expression fit expectations.

To further explore the nature of coexpression, we also considered the impact of eliminating deliberate μS PAS usage on the patterns of μS:mA and μM:mKO2 expression by introducing Irf4 and Blimp-1 mutations. μR mice were crossed to *Irf4*$^{-/-}$ and *Cd19*$^{+/Cre}$*Prdm1*$^{fl/fl}$ mice to examine μR expression patterns at homeostasis. Splenic CD19+F4/80- B cells from such mice exhibited similar coexpression of μM:mKO2 and μS:mA as wild type mice, **F1G**. As shown previously, these mice lacked PC in the spleen, **F1H,I**. This further corroborates our interpretation that μ GLT expression and/or stochastic CPA at the μS PAS leads to translation of a durable mA-H2B fusion protein. Thus, at homeostasis, μR B cells prevents a precise definition of μS expressing B cells and PCs.

Emergent plasmablasts produce graded patterns of μS PAS usage as well as the presence of distinct cell intermediates in μS PAS usage. Encouraged by the results in highly proliferative GCBs, we sought to determine whether we could visualize the dynamics of μS and μM PAS usage in the context of emergent plasmablast (PB) differentiation which requires multiple cell divisions.

LPS is a well-studied mitogen that promotes B cell activation, biosynthetic processes, cell cycle entry and division, upregulation of IRF4 and Blimp-1, PB differentiation, IgH and IgL upregulation, and preferential µS PAS usage. µR splenic B cells were enriched, labeled with Cell Trace Far Red (CTFR), and stimulated with LPS and cytokines (IL-2 and IL-5). Interestingly, as the cells underwent cell division at days 1 and 2 of culture, we observed sharp decrements of µM:mKO2 and µS:mA fluorescence that was present in naïve and undivided B cells, **F2A**. Between days 3-4, along with cell division, we observed acquisition of µS:mA expression that segregated into µS intermediate (µS INT) and µS high (µS HI) PAS usage states that were dim or negative for µM:mKO2 expression, respectively. In contrast, addition of IL-4 to the LPS cultures to induce CSR to IgG1 with concomitant deletion of the µ locus impaired µS:mA expression (**F2B**), consistent with its de novo production under these conditions. Furthermore, µS INT cells expressed abundant surface IgM protein and were depleted among surface IgM low cells, **SF3A**. In addition, switched cells, either de novo as in the case of IgG3 which is LPS-driven or from the splenic repertoire that proliferated with LPS were enriched among cells that were µS:mA negative, **SF3A**. Together, these observations support the use of an emergent PB differentiation system to visualize the dynamics of µS PAS usage. As Follicular B cells are not thought to be the main responders to LPS stimulation compared to MZ B cells, we performed the same experiment with purified B cells from lymph nodes which lack the MZ B cell subset and found that Follicular B cells achieved comparable µS INT and µS HI PAS usage rates (not shown) as that observed from splenic B cells. Similar dynamics were observed using CD40 Ligand and cytokines to mimic T-dependent responses (not shown) suggesting the observed dynamics are not unique to TLR stimulation. Thus, de novo production of graded µS PAS usage can be quantified during B cell activation and emergent PB differentiation.

To further explore the relationship of PB differentiation with the acquisition of μS INT and μS HI PAS usage states we bred μR mice to Prdm1:YFP mice in which YFP fluorescence reports on Blimp-1 expression[30]. Enriched μR Prdm1:YFP triple reporter B cells were labeled with Cell Trace Far Red (CTFR) and stimulated with LPS and cytokines. Interestingly, alongside cell division, two μS INT and two μS HI PAS states emerged that either expressed Prdm1:YFP or did not, **F2C**. Based upon the criterion of Blimp-1 expression in PB and for simplicity[13], we will refer to the Prdm1:YFP non-expressing populations as activated B cells (ActB) that are in either μS INT or μS HI PAS usage states and the Prdm1:YFP-expressing populations as PB that are in either μS INT or μS HI PAS usage states. To explore whether ActB μS HI cells derived from B1 precursor cells, during B cell enrichment we included anti-CD9 to our antibody depletion cocktail that already included anti-CD43 to deplete B1 and MZ B cells[31,32] and observed comparable μS INT and μS HI PAS usage rates suggesting that μS HI ActB cells are not exclusively B1 cell derived, **SF3B**. Lastly, to determine whether such cells differentiate in vivo, we used an adoptive transfer approach and transferred μR x Prdm1:YFP triple reporter splenic cells which are CD45.2 into congenic CD45.1 hosts and challenged with LPS to induce a T-Independent Type 1 response. Three days after challenge we observed all 4 populations as we observed in vitro, **SF3C**. As the μS:mA and Prdm1:YFP reporters accumulated and the μM:mKO2 reporter declined at similar rates, it was not possible to determine whether the kinetics of one reporter preceded that of the other, **F2D**.

μS PAS usage marks secreting cells. To confirm IgM secretory potential of μS INT and μS HI populations and to correlate them with distinct PB states, we measured Syndecan-1 (Synd1) expression in stimulated μR cells as well as Prdm1:YFP expression in μR x Prdm1:YFP cells. We observed that μS INT and μS HI cells could be ±Synd1, just as observed for Prdm1:YFP, **F3A**. To

confirm that μS INT and μS HI cells were secreting IgM, cells were sorted, plated onto filter plates for 5 hours, and actively secreting cells were counted using ELISpot. Interestingly, the μS INT Synd1- population contained slightly more secreting cells compared to the total Synd1- population, although this was not significant (see discussion). Notably, the μS HI Synd1- as well as the μS INT and μS HI Synd1+ counterparts contained as many secreting cells as that obtained by the total Synd1+ population sorted from control C57Bl/6 stimulated cells, **F3B**. However, contrary to the distinct expression levels of the μS:mA reporter, it was challenging to distinguish changes in secretion rates from inspection of spot sizes (data not shown). Thus, we turned to an IgM-specific ELISA approach where concentrations could be more easily quantitated. Following stimulation of μR x Prdm1:YFP cells, μS INT and μS HI ActB and PB populations were sorted and incubated in fresh media for an additional 5 hours before analyzing the supernatants, **F3C**. This revealed that μS INT ActB cells secrete more than Prdm1:YFP negative cells ($p \leq 0.0002$; t-test, unpaired) but ~3X fold less than μS HI ActB populations demonstrating that levels of μS:mA fluorescence expression correlates well with secretory capacity. Notably, secretory capacity of μS HI ActBs was comparable to that of PBs. -The greater fold difference in IgM secretion between Prdm1:YFP positive and Prdm1:YFP negative cells compared to the fold difference of ActBs that exhibit μS INT or μS HI PAS usage rates likely reflects that the ActB μS INT and μS HI populations comprise a minority of the overall Prdm1:YFP negative population. Cumulatively, μS:mA expression marks cells that are actively secreting IgM and that its graded expression reflects secretory competence.

IRF4 and Blimp-1 function hierarchically to promote μS PAS usage. To determine the relationship between the μS INT and μS HI PAS usage and the PB gene program, we stimulated μR x Prdm1:YFP B cells with LPS in the presence of anti-μ F(ab')2 which has been shown to antagonize LPS-dependent induction of Blimp-1 expression and μS PAS usage[33,34]. As previously

demonstrated, this condition efficiently prevented expression of Blimp-1 as measured using Prdm1:YFP, **F4A,B**. Notably, ActB µS HI PAS usage was inhibited but µS INT PAS usage was resistant to this condition. To further explore the regulation the of µS INT and µS HI PAS usage states, we bred the µR reporter to *Irf4*$^{-/-}$ and *Cd19*$^{+/cre}$*Prdm1*$^{fl/fl}$ mice. Splenic B cells were enriched from µR control (*Cd19*$^{+/cre}$) and mutant spleens and stimulated with LPS and cytokines. In contrast to the µS and µM PAS usage patterns observed in control LPS-stimulated B cells, analysis of parallel cultures of µR *Irf4*$^{-/-}$ and µR *Cd19*$^{+/Cre}$*Prdm1*$^{fl/fl}$ cells revealed that up- and down-regulation of µS and µM PAS usage, respectively, were impaired to differing extents, **F4C,D**. The residual µS HI cells of the *Cd19*$^{+/cre}$*Prdm1*$^{fl/fl}$ genotype likely comprises a mixture of incompletely deleted as well as µS HI ActB cells. Consistent with their hierarchical roles in PB differentiation, the transition from µM to µS PAS usage was more profoundly attenuated for the upstream regulator IRF4, **F4C,D**. To further quantify, we exported the fluorescence values of each cell and tabulated the µS:mA:µM:mKO2 ratios to estimate shifts in PAS usage. Binning the ratios revealed a hierarchical decrease in the ability of each TF to coordinate 3' end processing of the µ heavy chain primary transcript. *Irf4*$^{-/-}$ LPS-stimulated cells produced far fewer cells exhibiting ratios in the middle and top bins compared to such cells of the *Cd19*$^{+/cre}$*Prdm1*$^{fl/fl}$ genotype, which in turn lagged compared to the control genotype, **F4E**. These experiments further demonstrate the fidelity of graded µS:mA expression during cell division-linked PB differentiation. Remarkably, this single cell approach revealed for the first time that IRF4 and Blimp-1 function sequentially and non-redundantly to coordinate the µS to µM PAS usage ratios in activated B cells to those attained by PBs.

ActBs that exhibit graded µS PAS usage differ by distinct gene expression states but their PB counterparts do not. We next sought to determine the cell state basis of graded µS PAS usage by

transcriptome analysis. Following stimulation of µR x Prdm1:YFP cells, µS INT and µS HI ActB and PB populations were sorted and processed for RNA-seq. Quantification of the reads mapping to mA, mKO2, and YFP ORF sequences demonstrates the enrichments of the sorted populations. Importantly, it also demonstrates that transcript expression of the µS:mA reporter (i) is regulated at the transcriptional level and (ii) reflects fluorescent protein abundance. Together, this further demonstrates the reliability of µR expression patterns during emergent PB differentiation, **F5A-C**. In parallel, we sorted ±Prdm1:YFP populations from non-µR cells as a reference, ActB and PB cells, respectively. As expected, the transition to the PB state that is driven by IRF4 and Blimp-1 leads to profound changes in gene expression, **F5D**. Notably, ActB µS INT and µS HI populations exhibit differential gene expression, **F5E**. Upregulated genes are enriched for gene ontology terms relating to the endoplasmic reticulum and the Unfolded Protein Response (UPR), whereas downregulated genes are enriched for typical PB-related categories of antigen presentation and modulation of BCR signaling, **F5G**. In fact, in both the up- and down-regulated categories, a substantial portion is shared between those that accompany the Blimp-1-dependent transition to the PB state suggesting that µS HI ActB cells initiate key aspects of the PB gene program independently of Blimp-1 expression, **F5H**. In marked contrast, the µS INT and µS HI PB populations exhibited no statistically significant changes in gene expression, **F5F**. This suggests that these states may differ at the cellular rather than the genetic levels. Differential expression of each experimental sample was computed versus ActB cells from reference Prdm1:YFP negative cells, using a curated list of pro-PB, anti-PB, UPR, and Breg genes, **F5I**.This analysis highlights the less differentiated nature of µS INT ActB cells as well as the PB-like nature of µS HI ActBs. Lastly, we quantitated the µS to µM 3' mRNA read counts and their ratios to confirm that the differences in reporter expression was a result of alternate 3' end usage, **F5J-K**. Indeed, (i) lower

μS:μM ratios were evident among μS INT ActBs compared to all the other μR populations (ii) μS:μM ratios of μS INT ActB were higher than that of Prdm1:YFP negative cells (iii) μS:μM ratios among μS HI ActBs were comparable to that of μS INT and μS HI PB populations, and (iv) although indistinguishable μS:μM ratios are observed between μS INT and μS HI PB, the latter exhibited ~2X greater μS mRNA reads that is borderline significant (unpaired t-test; p=0.051). These differences in μS and μM mRNA levels further establishes the reliability of graded μS:mA reporter expression. Together, this analysis reveals the relatively undifferentiated status of intermediately secretory μS INT ActBs, that μS HI ActBs acquire key PB features independently of Blimp-1 expression, and that the gene program of μS INT and μS HI PB are indistinguishable.

Dynamic cell fate trajectories of μS INT and μS HI ActBs. Given the presence of multiple populations exhibiting graded μS PAS usage, we considered their cell fate trajectories as well as whether a given state(s) is fixed or dynamic. Following 3 days of stimulation of μR x Prdm1:YFP cells, ActB and PB that were either μS INT or μS HI were sorted, returned to culture with fresh medium for 23 hours, and reanalyzed, **F6**. Interestingly, μS INT and μS HI ActBs promptly generated PB counterparts. Furthermore, the ActB μS INT progenitors exhibited bi-potential cell fate trajectories and could bypass Blimp-1 expression to give rise to ActB μS HI progeny. In contrast, the μS INT and μS HI PB populations exhibited weak progenitor potential. Importantly, these experiments reveal that μS HI PB derive from μS HI ActB rather than from μS INT PB precursors, highlighting a distinct cellular intermediate in μS PAS regulation and PC differentiation.

Graded PAS usage correlates with distinct cell biological states. Given the paucity of gene expression differences between the μS INT and μS HI PB populations, we considered whether cell biological features may differentially correlate with Blimp-1 expression and graded μS PAS usage.

We considered three categories: (**F7A**) B cell identity including expression of µM:mKO2, Pax5, and CD22, (**F7B**) classical PB definitions including Synd1 and IRF4 expression, and (**F7C**) basic cell biological properties including translation efficiency (O-Propargyl-puromycin, OPP) and ER biomass (ER Tracker). Similar to the above observations, the µS INT ActB population, that as a group were moderately secretory, exhibited the greatest heterogeneity with respect to B cell identity and PB fate trajectories in that it was bimodal for µM:mKO2, CD22, Pax5, Synd1, and IRF4 high. Bimodality indicates a mixed population where some cells retain properties of B cells and others may be early PB, consistent with the lower secretory capacity of ActB µS INT cells, **F4**. In contrast, the µS HI ActB population clearly downregulated µM:mKO2, Pax5, and CD22 and upregulated Synd1 and high IRF4 expression, suggesting a definitive PB fate trajectory. Both the µS INT and µS HI PB populations also clearly exhibited features of the PB state, as expected. With regards to cell biological features, all populations displayed equivalent gMFI of OPP, suggesting comparable translation efficiencies. Notably, transitioning from µS INT ActB to all other µS populations was associated with a graded increase in gMFI of ER Tracker dye whereby the µS INT and µS HI PB displayed the largest ER biomass, **F7C**. Furthermore, inspection of genes differentially expressed between the ActB µS INT to either PB µS HI or to ActB µS HI transitions revealed that the gene ontology category endoplasmic reticulum (GO:0005783) was commonly enriched. Strikingly, however, a fraction of those genes did not overlap and displayed preferential expression depending on the cell fate trajectory, **F7D**. Together, these results reveal the relatively less mature PB-like state of the µS INT ActB cells and demonstrate that their transition into µS HI ActB or µS INT PB is associated with loss of B cell identity features, greater PB maturity, and increases in ER biomass. Notably, preferential expression of ER-associated genes

characterizes the cell fate choice of μS INT ActBs, suggesting differential functional derivatization of ER biogenesis according to cell fate trajectories.

Discussion

Using B cells from a novel reporter mouse of the IgH μ locus, we have demonstrated the presence of an unpredicted developmental intermediate in the deployment of graded μS PAS usage in B cells undergoing the transition to a secretory state and PB differentiation. This was possible because we developed a novel dual fluorescent protein reporter mouse to quantify, at the single cell level, differential usage of the μS and μM PAS elements responsible for 3' end processing of the μ primary transcript. μReporter mice displayed normal amounts of all B cell subsets and expression of the reporters were prominently expressed in B cells and nominally expressed in non-B cells that are known to express GLT of μ[27]. However, at homeostasis, we were surprised to observe that μR splenic B cells coexpressed high amounts of μS:mA with μM:mKO2 despite reports that antibody secreting cells are rare[14]. We suspect that this false-positive pattern may reflect ongoing translation of μ GLT[28] and/or stochastic usage of μS PAS combined with durability of the mA fluorescent protein expression. This interpretation was substantiated by observing similar coexpression patterns of μR at homeostasis on the Irf4 and Blimp-1 mutant backgrounds where deliberate μS PAS usage is prevented as well as analysis of ex vivo IgG1 switched cells. In contrast, we were encouraged that non-secretory, highly proliferative and highly catabolic GCBs expressed negligible levels of μS:mA suggesting that some cell conditions could yield reliable and biologically relevant μR expression.

Inspired by the μR expression pattern in such GCBs, we reasoned that μR expression dynamics could be visualized in activated B cells. In an emergent PB culture system we observed de novo

production of graded μS:mA expression in a division-linked manner. In fact, graded transcript abundance of μS and μS:mA demonstrates that the differences in fluorescence intensity are driven at the transcriptional level. We confirmed that this pattern of expression represented bona fide secreting cells by sorting μS INT and μS HI-expressing cells that were or were not expressing Synd1, as well as control C57Bl/6 ±Synd1 cells and measured secreted IgM by ELISpot. Except for the many that were counted from μS INT Synd1 negative cells, we observed spot-forming efficiencies in μS HI-expressing Synd1 negative cells that matched that observed using Synd1-expressing μS INT, μS HI, and C57Bl/6 control cells. The transcriptome and cell biological measurements of the μS INT ActB population suggest that the lower spot-forming efficiency of this population is due to their mixed B/PB nature and underdeveloped secretory apparatus (discussed below). Importantly, abundance of secretory IgM in supernatants of sorted μS INT and HI ActB populations correlated with fluorescent protein intensities demonstrating the power of the μR allele. This point is underscored by lower and higher μS:μM mRNA ratios quantitated between μS INT and μS HI ActB populations, respectively, which demonstrates that fluorescent protein expression reflects differences at the level of mRNA. Moreover, transcript abundance of the fluorescent genes tracked with fluorescent intensities. Notably, upregulation of Blimp-1 in μS INT cells resulted in efficient IgM secretory competence, likely due to Blimp-1's role in coordinating both enhanced μS PAS usage and UPR activity. Curiously, despite differences in reporter expression and IgM transcript abundance, μS INT and μS HI PB did not differ in the magnitude of IgM secretion (discussed below). Together, catabolic conditions during B cell activation and emergent PB differentiation revealed the differentiation of activated B cells with variegated μS PAS usage and IgM secretory competence.

We confirmed that graded μS expression was predictably regulated by employing established stimulation conditions that diminish or eliminate μS PAS usage. In the first, LPS co-stimulation with α-IgM F(ab')2 has been shown to prevent the upregulation of Blimp-1 and attendant μS PAS usage[33,34]. Indeed, expression of the Prdm1:YFP reporter decreased substantially and was associated with diminished μS PAS reporter expression in these stimulation conditions. In the second, we reasoned that deletion of the μ locus by CSR should diminish reporter expression. Indeed, ex vivo IgG1 cells exhibited no μR expression and those undergoing de novo IgG1 switching by stimulation with LPS in the presence of IL4 resulted in decreased μS INT and no μS HI PAS usage. We suspect that the residual INT μS:mA expression derived from activated B cells prior to CSR. In the third, we used a genetic approach and bred μR mice to *Irf4*$^{-/-}$ or to *Cd19*$^{+/Cre}$*Prdm1*$^{fl/fl}$ backgrounds with the expectation that preventing PB differentiation and attendant changes in μS:μM mRNA ratios would lessen graded μS PAS usage. Indeed, both backgrounds prevented (*Irf4-/-*) or attenuated (*Cd19+/CrePrdm1fl/*fl) graded μS PAS usage. Together, these signaling and genetic perturbations demonstrate that only under conditions of established IgM secretory competence is graded μS PAS reporter expression observed.

Importantly, the distinct acquired patterns of μS and μM PAS usage observed between the IRF4 and Blimp-1 mutant backgrounds delineate the non-redundant roles that these hierarchical PB fate determinants play in μ RNA biosynthesis and post-transcriptional regulation. Specifically, we conclude that IRF4 boosts overall expression of μ, upon which, Blimp-1 further augments and directs preferential μS PAS usage. Regarding the latter mutation, a residual population of μS HI cells persist, likely as a mixture of undeleted cells as well as Blimp-1-independent secretors, here and Savage et. al.[14]. The IgH 3' enhancer, a multipartite super-enhancer, is essential for both CSR as well as for boosting IgH mRNA synthesis in PC[35]. In fact, both IRF4 and Blimp-1 occupy

regions and control accessibility of the IgH 3' enhancer[36]. The analysis herein suggests that their functional activities on the IgH 3' enhancer are distinct. Specifically, in *Irf4*$^{-/-}$ B cells, germline transcription of γ1 as well as efficient restoration of γ1 CSR upon AID complementation indicates that aspects of the IgH 3' enhancer are accessible and active[20]. Thus, we speculate that the effects of the IgH 3' enhancer on CSR and IgH expression are governed by separable modules.

To correlate graded μS PAS usage with activated and differentiated B cell states, we bred a third reporter allele encoded by a Prdm1:YFP BAC. This experiment was particularly informative as it revealed four cellular populations that emerged upon B cell activation and differentiation; μS INT and μS HI ActB that did not express Prdm1:YFP as well as μS INT and μS HI PB counterparts that did express Prdm1:YFP. Notably, such cells were also observed in vivo following T-independent type 1 challenge. Also, depleting B1 cells prior to in vitro stimulation continued to generate μS HI ActB cells, demonstrating that these cells are not exclusively B1. The μS ActB population is the least differentiated based on lower IgM secretion capacity, sustained usage of μM PAS, lower μS:μM mRNA ratios, a greater anti-PB accompanied with weaker pro-PB gene program, resistance to inhibition by LPS with αIgM F(ab')2 co-stimulation, high PB progenitor potential as well as cell biological parameters that include an under-developed ER. In addition, despite detectable μS PAS usage, this population appears heterogenous with bimodal expression of Pax5/CD22 and IRF4/Synd1. In contrast, the other three populations, μS HI ActB as well as the μS INT and μS HI PB counterparts, all display features of differentiated PBs including diminished μM PAS usage, higher μS:μM mRNA ratios, sensitivity to inhibition by LPS with αIgM F(ab')2 co-stimulation, high expression of a pro-PB and decreased expression of the anti-PB gene program, high expression of UPR component genes, and increased ER biomass. Thus, the combination of increased μS PAS usage and a PB-like gene program attendant with enhanced UPR and ER

biomass enables μS HI ActB to efficiently secrete IgM. Moreover, these observations highlight that aspects of the PC gene program occur independently of Blimp-1 activity. These observations are in line with an earlier report that Blimp-1 is not required for some PC to secrete high levels of IgM[14].

ActB and PB populations displaying graded μS PAS usage accumulated at similar rates as a function of the number of cell divisions experienced following stimulation preventing an opportunity to determine progenitor-progeny relationships. However, upon isolation and re-culture, we observed dynamic cell flux for the μS INT and μS HI ActB and comparatively static cell fate trajectories for the μS INT and μS HI PB counterparts. Specifically, both the μS INT and μS HI ActB efficiently acquired Prdm1:YFP expression. Interestingly, μS INT ActB cells exhibited bipotential cell fate trajectories as they also attained μS HI ActB status. In contrast, the μS INT PB counterpart did not quantitatively acquire μS HI status during the same period. Nor did either of the PB populations lose Prdm1:YFP expression consistent with the notion that Blimp-1-expressing PB are terminally differentiated. We note that we were limited to a single day of re-culture given the short-term properties of LPS stimulations. Thus, assent to the μS HI PB state occurs via a distinct intermediate that displays increased μS PAS usage rates independently of Blimp-1 expression.

The progenitor – progeny experiment reveals two notable observations evident in the μS INT ActB and PB counterpart. The latter PB population does not readily generate μS HI PB during the period of analysis. In contrast, the μS INT ActB counterpart exhibits bi-potentiality and undergoes a cell fate choice to either (i) maintain μS INT PAS usage and acquire Blimp-1 expression or (ii) increase μ abundance and μS PAS usage without concomitant Blimp-1 expression. We speculate these cells experience two rates of Prdm1 gene activation, slow and fast, mediated by the rate of increase in

activity of the pro-PB transcription factor IRF4 or decrease of anti-PB regulatory transcription factor activity (e.g. Pax5, Bach2). The µS HI ActB progeny express uniform high IRF4 expression suggesting that the transition from µS INT to µS HI ActB is driven in part by increased activity of IRF4; however, given that Prdm1 is a direct target gene of IRF4 it remains unclear why this occurs without concomitant activation of Blimp-1 expression. Future experiments will determine whether the Prdm1 locus exhibits distinctive rates of epigenetic remodeling that could underlie this cell fate choice.

Despite similar gene expression profiles, comparable µS:µM mRNA ratios, and comparable secretory IgM capacity, notable differences exist between µS INT and µS HI PB. First, along with the differences in µS:mA expression, µS HI PB express more µS transcript expression (as well as mA transcripts), suggesting a greater propensity for µ mRNA biosynthesis compared to µS INT PB. This, combined with the comparable µS:µSM mRNA ratios between µS INT and µS HI PB suggests that the latter should secrete more IgM; however, this was not observed. Future experiments are needed to determine if the lack of enhanced secreted IgM from µS HI PB is because of greater Endoplasmic Reticulum Associated Degradation (ERAD) due to the higher IgM payload (Ricci et al., 2021). Second, the µS INT and µS HI PB arise from distinct precursor cells. µS INT PB derive from µS INT ActB whereas µS HI PB arise from the distinct intermediate found using µR mice, µS HI ActB, which in turn stemmed from the µS INT ActB progenitors. The relevance of this developmental pathway remains to be determined but one possibility is that, given increased expression of ER- and UPR- associated genes as well as attendant changes in ER biomass during the transition of µS INT to µS HI ActB, perhaps the fate of ER shape, biogenesis, or activity evolves distinctly from that remodeled by increased Blimp-1 during the transition from µS INT ActB to the µS INT PB counterpart. In support of this, differential expression of ER-

associated genes is evident that distinguishes the forked cell fate trajectories. We speculate that these mechanisms have evolved to enable differential remodeling of ER function between the μS INT and μS HI PB. Notably, ER biomass is further increased during the transition from μS HI ActB to μS HI PB as these cells acquire Blimp-1 expression raising the possibility of greater sophistication of the ER sheet and tubular network or functionality. Future experiments will probe whether the two modes of ER maturation experienced by the μS INT and μS HI PB imprint differences in the kinetics of the folding and assembly of disulfide-bonded IgM heterodimers, differential polymerization of heterodimers, glycosylation, or quality control activity including ERAD. We note that the idea that distinct lineage-restricted progenitors give rise to progeny exhibiting distinctive functional qualities is not new as evidenced by B1 and B2 cell progenitors that give rise to mature B1 and B2 cells that play differential roles in the antibody response[37].

Limitations of the study

Our analysis points to coordination of low and high μS PAS usage with distinct ActB and PB cell states during emergent PB differentiation in vitro and in vivo. Some of these observations were predicted from numerous experiments that demonstrated variable spot sizes of antibody secreting cells using ELISpot experiments. Although we demonstrate that ActB μS INT and HI cells exhibit progenitor potential, the short time frames of in vitro stimulated cells prevents us from quantifying those rates and efficiencies. We have highlighted the role of μ GLT and its translation in limiting the use of the μR mice in various settings.

Resource availability

Lead contact:

Roger Sciammas (rsciammas@ucdavis.edu) should be contacted for further information and request for resources.

Materials availability:

Further information and requests for resources and reagents should be directed to and will be fulfilled by Yongsheng Shi (yongshes@uci.edu) and Roger Sciammas (rsciammas@ucdavis.edu). The µReporter mice described here are available upon request to the Lead contact and a completed Materials Transfer Agreement.

Data and Code availability:

- RNA-seq data has been deposited into NCBI GEO as accession GSE242335.
- This paper does not report original code.
- No other standardized Data has been generated.

Acknowledgements

We thank members of the Sciammas and Shi labs for discussions. Flow cytometry and sorting was supported by the Flow Cytometry Core of the California National Primate Research Center under NIH award number P51OD011107. This work was supported in part by R01 AI170840 (to RS & YS) and R21 AI151610 (to RS).

Author contributions

Evelyn Sievert: Data curation; formal analysis; validation; investigation; visualization; methodology; writing – review and editing. Marissa Franke: Data curation; formal analysis; validation; investigation; visualization; methodology; writing – review and editing. Kayla

Thomas: Data curation; formal analysis; validation; investigation; visualization; methodology; writing – review and editing. Yoseop Yoon: Data curation formal analysis; validation; investigation; visualization; methodology; writing – review and editing. Yongsheng Shi: Conceptualization; data curation; supervision; funding acquisition; investigation; visualization; writing – original draft; project administration; writing – review and editing. Roger Sciammas: Conceptualization; data curation; supervision; funding acquisition; investigation; visualization; writing – original draft; project administration; writing – review and editing.

Declaration of interests

Authors declare no Conflicts of interest.

Main figure titles and legends

Figure 1. Generation of µR mice that encode dual fluorescent reporters to enumerate B cells undergoing alternative µM and µS PAS usage. See also SF1, 2.

A. Schematic depicting the splicing and 3' end processing activities on the µ primary transcript. PAS denotes poly-adenylation site. Abbreviations: PAS, polyadenylation sequence; CPA, Cleavage and Polyadenylation; m^7G, 5' methylated guanosine cap; pA, polyadenylation tail; prox, proximal; dist, distal.

B. Schematic depicting the targeting approach.

C. Patterns of µR reporter expression among splenic B220+ cells from non-fluorescent C57Bl/6 or µR mice. Representative of at least 3 independent experiments.

D. Patterns of µR reporter expression among splenic B220+ cells in relation to surface IgM or among CD4/CD8+ ex vivo cells. Contour plots are overlayed with that of non-fluorescent C57Bl/6 control splenic cells. Representative of at least 3 independent experiments.

E. Patterns of µR reporter expression among ex vivo splenic B220+IgG1+ or B220+IgM+ cells. Left, gating strategy and right expression patterns of cells within each gate of µR or C57Bl/6 mice. Representative of 2 independent experiments.

F. Pattern of µR reporter expression in B220+IgD-CD38loFas+ splenic B cells. Contour plot is overlayed with that of non-fluorescent C57Bl/6 control GC B cells. Representative of 3 independent experiments.

G. Patterns of µR reporter expression in splenic B cells (B220+) from mice of indicated genotype. Contour plot is overlayed with that of non-fluorescent C57Bl/6 splenic B cells.

H. Frequencies of splenic Plasma cells (CD19hi/loCD4-F4/80-Sca1+Synd1+) from mice with indicated genotypes.

I. Quantitation of frequencies of panel B. Each point represents an independent biological replicate from two mice and error bars represent ±SD of the mean.

Figure 2. B cell stimulation results in de novo µR reporter expression that display graded µS PAS usage. See also SF3.

A. Analysis of µR reporter expression in relation to cell division using Cell Trace Far Red (CTFR) at indicated days following LPS and IL2/5 stimulation. Contour plot is overlayed with that of similarly treated non-fluorescent C57Bl/6 splenic B cells. Representative of 3 independent experiments. Live, DAPI-excluded cells are shown.

B. Analysis of µR reporter expression in IgM (IgG1 negative) or in IgG1+ cells 3 days after stimulation with LPS and IL4. Live, DAPI-excluded cells are shown. Control represents similarly treated non-fluorescent C57Bl/6 cells. Representative of 3 independent experiments.

C. Analysis of μR reporter expression in relation to cell division and Prdm1:YFP reporter expression after four days of LPS and IL2/5 stimulation. Live, DAPI-excluded cells are shown. Contour plot is overlayed with that of similarly treated non-fluorescent C57Bl/6 cells. The gates depicted in the right most panel uses the C57Bl/6 fluorescent intensity to exclude cells that are not expressing μR. Representative of at least 3 independent experiments.

D. Histogram depicting the gates of mathematically computed divisions among live, DAPI-excluded cells, left. Line graph quantifying the changes of μR and Prdm1:YFP reporter expression in each division, right. Distribution of μR and Prdm1:YFP reporter expression within indicated cell divisions, bottom. Gates with corresponding frequencies represent ActB μS INT, ActB μS HI, PB μS INT, and PB μS HI. Representative of 3 independent experiments.

Figure 3. μS:mA expression marks secreting cells.

A. Analysis of μR reporter expression in relation to Synd1 expression (top) and Prdm1:YFP expression (bottom). Gates with corresponding frequencies represent ActB μS INT, ActB μS HI, PB μS INT, and PB μS HI among live, DAPI-excluded cells. Contour plot is overlayed with that of similarly treated non-fluorescent C57Bl/6 cells. Representative of 3 independent experiments.

B. ELISpot measurement of IgM-secreting cells from sorted cells as a function of graded μS PAS usage and Synd1 expression. 100 cells from each gate were sorted into filter plates and cells were cultured for 5 hours. Each spot on the bar graph represents a replicate measurement in a given experiment and error bars represent ±SD of the mean. Result is representative of five independent experiments.

C. ELISA measurement of IgM secretion from sorted cells as a function of graded μS PAS usage and Prdm1:YFP expression, left. Fold change between indicated groups, right. 25,000 cells were sorted, and cells were cultured for 5 hours before cell-free supernatants were harvested. Results from three independent experiments are depicted by dots on bar graph and error bars represent ±SD of the mean. For reference, similarly treated Prdm1:YFP only cells were analyzed.

Figure 4. Signaling or genetic inhibition of PB differentiation prevents graded μS PAS usage.

A. Analysis of μR and Prdm1:YFP expression in conditions of LPS only or LPS with α-IgM F(ab')2, at four days after stimulation. Gates with corresponding frequencies represent ActB μS INT, ActB μS HI, PB μS INT, and PB μS HI among DAPI-excluded live cells. Contour plot is overlayed with that of similarly treated non-fluorescent C57Bl/6 cells.

B. Quantitation of panel A where each point represents an independent biological replicate and error bars represent ±SD of the mean.

C. Analysis of μR reporter expression at four days following LPS and IL2/5 stimulation using B cells of indicated genotypes. Analysis excludes dead cells and includes only cells exhibiting ≥2 cell divisions. Gates with corresponding frequencies represent μS INT and μS HI cells. Contour plot is overlayed with that of similarly treated non-fluorescent C57Bl/6 cells.

D. Quantitation of panel C where each point represents a biological replicate and error bars represent ±SD of the mean.

E. Quantitation of cell frequencies within bins of µS:mA to µM:mKO2 ratios of fluorescence intensities among cells of indicated genotypes. Greater or equal to 16,000 events analyzed per genotype. Each dot represents the results obtained in independent biological experiments and error bars represent ±SD of the mean.

Figure 5. Transcriptional differences associated with graded µS PAS usage and Prdm1:YFP expression.

A. Box plot quantifying RNA-seq read counts (Log2) mapping to the mA open reading frame in ActB µS INT, ActB µS HI, PB µS INT, PB µS HI as well as ActB and PB populations from reference Prdm1:YFP only cells. Not Detected (N.D.). RNA-seq data was computed using 2 or 3 replicates per group and error bars represent ±SD of the mean.

B. Box plot quantifying RNA-seq read counts (Log2) mapping to the mKO2 open reading frame in ActB µS INT, ActB µS HI, PB µS INT, PB µS HI as well as ActB and PB populations from reference Prdm1:YFP only cells. Not Detected (N.D.). RNA-seq data was computed using 2 or 3 replicates per group and error bars represent ±SD of the mean.

C. Box plot quantifying RNA-seq read counts (Log2) mapping to the YFP open reading frame in ActB µS INT, ActB µS HI, PB µS INT, PB µS HI as well as ActB and PB populations from reference Prdm1:YFP only cells. Not Detected (N.D.). RNA-seq data was computed using 2 or 3 replicates per group and error bars represent ±SD of the mean.

D. Volcano Plot of differentially expressed genes between ±Prdm1:YFP only cells. Yellow box highlights upregulated genes by ≥2 fold differences and a false discovery rate ≤0.05. Blue box features downregulated genes by ≥2 fold differences and a false discovery rate ≤0.05.

E. Volcano Plot of differentially expressed genes between µS INT and µS HI ActB, depicted as in D.

F. Volcano Plot of differentially expressed genes between µS INT and µS HI PB, depicted as in D.

G. List of top gene ontology categories in the µS INT to µS HI populations that are both Prdm1:YFP negative. Yellow box includes upregulated and blue box includes downregulated categories. Numbers indicate p-value of enrichment.

H. Venn diagram depicting the number of unique as well as shared differentially expressed genes between the two indicated pairwise comparisons; top row is for upregulated and bottom row is for downregulated genes.

I. Heat map depicting changes of select genes that promote the PB gene program, antagonize the PB gene program, are involved in Unfolded Protein Response (UPR), or are attendant with the Breg cell state. All pairwise comparisons are to the ActB cells (YFP-) from the Prdm1:YFP only mouse.

J. RNA-seq tracks depicting read counts (FPKM) at the 3' of the µ locus. Box highlights the µS exon and row numbers show mean and standard deviation of µS read counts.

K. Box plot depicting µS:µM ratios calculated from the RNA-seq read counts among the indicated samples. RNA-seq data was computed using 2 or 3 replicates per group and error bars represent ±SD of the mean.

Figure 6. Progenitor fate trajectories of graded μS cells that are Prdm1:YFP expressing or not.

A. Each row presents the results of the indicated sorted and recultured populations among DAPI-excluded cells. Column on the left shows each progenitor population immediately after cell sorting (three days of LPS and cytokine stimulation) and the column in the middle shows the fate of those cells after 23 hours of subsequent culture. The boxes indicate the percentages of cells in each gate. Quantification of the fold gain of the percentage of cells in a given gate before and after 23 hours of culture is shown in the right column. Percentages were changed to 1 if their value was less than 1. Each point represents an independent biological experiment and error bars represent ±SD of the mean. Asterisks represent $p<0.05$ calculated using an unpaired t-test.

Figure 7. Expression of cell biological, B lineage, PB features or ER associated genes among graded μS populations that express Prdm1:YFP or not.

A. Histograms depicting expression of designated biological lineage parameters in indicated populations among DAPI-excluded cells; each column presents the results of μM, Cd22, or Pax5 expression. Bar graphs at the bottom depict percent of cells expressing given marker in each population and each dot represents an independent biological replicate and error bars represent ±SD of the mean. Asterisks indicate ≤0.05 unpaired t-test result between bracketed populations.

B. Histograms depicting expression of designated PB parameters in indicated populations; each column presents the results of Synd1 and IRF4 expression. Bar graphs at the bottom depict percent of cells expressing given marker in each population and each dot represents an independent biological replicate and error bars represent ±SD of the mean. Asterisks indicate ≤0.05 unpaired t-test result between bracketed populations.

C. Histograms depicting expression of designated cell biological parameters in indicated populations; each column presents the results of O-propargyl puromycin (OPP) biosynthetic labeling and ER-Tracker staining. The bar graphs at the bottom of OPP column depicts gMFI. The bar graph at the bottom of ER-Tracker column depicts fold change in gMFI compared to ActB μS INT cells and each dot represents an independent biological replicate and error bars represent ±SD of the mean. Asterisks indicate ≤0.05 unpaired t-test result between bracketed populations.

D. Heat map depicting the change of expression among genes assigned to the gene ontology group GO:0005783 Endoplasmic Reticulum that was commonly enriched in the ActB μS INT to ActB μS HI transition (blue font) and in the ActB μS INT to PB μS INT transition (red font). Xbp1, also in GO:0005783, was enriched in both transitions. We note that genes Faah, Hap1, Itga5, Tpp2, Wfs1, Cln8, Ggcx, Dnajb2, Rsad2, Asph, Derl3, Atp6ap2, Sil1, Kdel3, Tlr7 (ActB μS INT to ActB μS HI) and genes Dnajb9, Edem3 (ActB μS INT to PB μS INT) are formally considered differentially expressed in the respective data sets; however, they were excluded from the figure because they did not pass the differential expression and/or FDR cutoffs evident in the contrasting pairwise comparison.

STAR★Methods

Key resources table

REAGENT or RESOURCE	SOURCE	IDENTIFIER
Antibodies		
anti-CD4 biotin	BD Pharmingen	RRID:AB_394580
anti-CD8 biotin	BD Pharmingen	RRID:AB_394566
anti-CD3 biotin	BD Pharmingen	RRID:AB_394728
anti-CD43 biotin	BD Pharmingen	RRID:AB_394581
anti-CD49b biotin	BD Pharmingen	RRID:AB_395092
anti-Gr1 biotin	BD Pharmingen	RRID:AB_394641
anti-CD11b biotin	BD Pharmingen	RRID:AB_394773
anti-Ter119 biotin	BD Pharmingen	RRID:AB_394985
anti-CD9 biotin	BD Pharmingen	RRID:AB_397103
anti-CD22 biotin	BD Pharmingen	RRID:AB_394823
anti-CD138 APC	BD Pharmingen	RRID:AB_1645216
anti-IRF4 PE-Cy7	eBioscience	RRID: AB_2573558
anti-B220 PE-Cy7	BD Pharmingen	RRID:AB_394458
anti-CD19 APC-Cy7	BD Pharmingen	RRID:AB_10896279
anti-IgD PerCP-Cy5.5	BD Pharmingen	RRID:AB_2738722
anti-CD4 Pacific Blue	Biolegend	RRID:AB_493646
anti-CD23 AF647	BD Pharmingen	RRID:AB_2737821
anti-CD21 BV421	BD Pharmingen	RRID:AB_2737772
anti-F4/80 BV421	BD Pharmingen	RRID:AB_2734779
anti-Sca1 PE-Cy7	BD Pharmingen	RRID:AB_647253
anti-Fas PE-CF594	BD Pharmingen	RRID:AB_11154214
anti-CD38 APC-Cy7	Biolegend	RRID: AB_2616967
anti-CD45.1 BV421	BD Pharmingen	RRID:AB_2738523
anti-CD45.2 APC-Cy7	BD Pharmingen	RRID:AB_1727492
anti-CD16/32	Bio X Cell	RRID:AB_2736987
anti-IgMb biotin	BD Biosciences	RRID:AB_394900
anti-IgG1 biotin	BD Biosciences	RRID:AB_2296342
anti-IgG2a biotin	BD Biosciences	Cat #553388
anti-IgG2b/c biotin	BD Biosciences	RRID:AB_393613
anti-IgG3 biotin	BD Biosciences	RRID:AB_394838
SAv AF647	ThermoFisher	Cat #S-21374
AffiniPure Goat Anti-Mouse IgG, F(ab')$_2$ fragment specific (min X Hu, Bov, Hrs Sr Prot)	Jackson Immunoresearch	RRID: AB_2338455
AlkPhosph AffiniPure Goat Anti-Mouse IgG, Fcγ Frag Spec (min X Hu,Bov,Hrs Sr Prot	Jackson Immunoresearch	RRID: AB_2338535
AlkPhosp AffiniPure Goat Anti-Mouse IgM, μ Chain Specific (min X Hu,Bov,Hrs Sr Prot)	Jackson Immunoresearch	RRID: AB_2338537
Chemicals, peptides, and recombinant proteins		
rhIL2	NCI	
rmIL5	Peprotech	Cat #215-15
Cell Trace Far Red	ThermoFisher	Cat #ECd3472

ER-Tracker™ Red (BODIPY™ TR Glibenclamide	ThermoFisher	Cat #E3425
DAPI	Molecular Probes	Cat #D1306
Live/Dead Fixable Blue	Life Technologies	Cat #15596-018
Trizol	Invitrogen	Cat #15596018
Lipopolysaccharides from Salmonella enterica serotype typhimurium; purified by trichloroacetic acid extraction	Sigma-Aldrich	Cat #L7261
Lipopolysaccharide from Salmonella minnesota R595 (Re); 1mL	Enzo Biosciences	Cat #ALX-581-008-L001
Iscove's Modified Dulbecco's Medium; liquid, sterile-filtered, With sodium bicarbonate, without L-glutamine, suitable for cell culture, suitable for hybridoma	Sigma-Aldrich	Cat #I3390
FBS	GenClone	Cat #25-514
Hepes buffer		Cat #H0887
NEAA	Sigma-Aldrich	Cat #M7145
Gibco 2-Mercaptoethanol	ThermoFisher	Cat #21985023
Sodium Pyruvate	Sigma-Aldrich	Cat #S8636
Glutamax	ThermoFisher	Cat #35050061
Penicillin/Streptomycin	Sigma-Aldrich	Cat #P4333
anti-BIOTIN microbead UltraPure	Miltenyi	Cat #130-105-637
LS Columns	Miltenyi	Cat #130-042-401
Critical commercial assays		
TruSeq Stranded mRNA Library Prep kit	Illumina	Cat #20020595
eBioscience™ Intracellular Fixation & Permeabilization Buffer Set	ThermoFisher	Cat #88-8824-00
Click Chemistry Tools; Click-&-Go® Plus 647 OPP Protein Synthesis Assay Kit	Click Chemistry Tools	Cat #1496
Deposited data		
RNA-seq, NCBI GEO accession GSE242335	This study	GSE242335
Experimental models: Cell lines		
C57BL/6 ES cell line, Bruce4 (Köntgen et al., 1993)		Ozgene Pty Ltd
Experimental models: Organisms/strains		
µReporter	This study	
C57BL/6 µReporter littermate	This study	
B6.Cg-Tg(Prdm1-EYFP)1Mnz/J	Jackson Labs	Strain #008828
pB6.SJL-Ptprca Pepcb/BoyJ	Jackson Labs	Strain #002014
Primary B cells	This study	
Recombinant DNA		
µReporter targeting construct	This study	Ozgene Pty Ltd
Software and algorithms		
Cutadapt (Martin, 2011)		
STAR (Dobin et al., 2013)		
edgeR (Robinson et al., 2010)		

Experimental model and study participant details

The *Igh6* knock-in mouse line, µR herein, was generated by Ozgene Pty Ltd (Bentley WA, Australia). P2A_mA:H2b was knocked in place of the STOP codon at position chr12:114659080-114659078 of the mouse genome (mm9 assembly) and IRES_mKusabira-Orange 2 after STOP codon at position chr12:114657036-114657037 of the mouse genome (mm9 assembly). The µS PAS is tagged by monomeric Ametrine (mA) which exhibits excitation/emission of 406/526λ following excitation by the violet laser (405λ) whereas the µM PAS is tagged by monomeric Kusabira Orange 2 (mKO2) which displays excitation/emission of 551/565λ following excitation by the yellow/green laser (532λ). Each of these were encoded to produce bicistronic transcripts: for the µS PAS, we introduced sequence encoding the 18 amino acid P2A from Teschovirus which causes ribosomal skipping during translation and poly-protein production of secreted µ and mA; for the µM PAS, we introduced an IRES sequence to prevent ribosomal release and poly-protein production of membrane µ and mKO2. This design links the expression of the fluorescent proteins to µ PAS usage and translation of the µS and µM proteins. To enable isolation and interrogation of nuclei we fused mA to Histone2B to trap the fluorescent protein in nuclear chromatin. Finally, as the Neomycin selection expression unit is known to affect the Ig locus by transcriptional interference[38], it was flanked with frt sites for Flpe-dependent excision. The construct was electroporated into Bruce4 ES cells, drug selected, and clones were identified by PCR, **SF1**. Targeted ES cells were used to produce mice which we term µReporter or µR mice. µR mice were then crossed to Flpe transgenic mice to remove the Neomycin selection expression unit. The targeting construct was electroporated into a C57BL/6 ES cell line, Bruce4[39]. Homologous recombinant ES cell clones were identified by qPCR and injected into goGermline blastocysts[39]. Male chimeric mice were obtained and crossed to C57BL/6J FLP females to remove the FRT

flanked selectable marker cassette and to establish heterozygous germline offspring on C57BL/6 background.

The generation and genotyping of the *Irf4-/-* mice has been previously described and the mice have been extensively backcrossed to the C57Bl/6 background[40]. The *Cd19*$^{+/Cre}$ (006785), *Prdm1*$^{fl/fl}$, (008100) and Prdm1:YFP (008828) mice were from The Jackson Laboratory and genotyped using JAX protocols[30,41,42]. B6.SJL-Ptprca Pepcb/BoyJ (0006584) from JAX were bred in house. µR mice were genotyped using PCR and a three-set primer mixture that distinguishes heterozygous from wild type and homozygous mice, **SF1**. No influence (or association) of sex, gender, or both on the results of the study is reported. Mice were housed in specific pathogen-free conditions and were used and maintained in accordance with the Institutional Animal Care and Use Committee guidelines at UC Davis.

Method details

Cells and culture conditions

Splenic B cells were isolated by sequential hypotonic lysis and magnetic bead separation. Briefly, a single cell suspension of spleen cells was treated with Tris buffered ammonium chloride to lyse red blood cells and then a negative selection, bead-based immunopurification strategy was employed that depletes T, NK, and macrophage cells using a cocktail of biotinylated antibodies specific for CD4, CD8, CD3, CD43, CD49b, Gr1, CD11b, Ter119 (BD Biosciences) and adsorption to Streptavidin microbeads (Miltenyi Biotec Inc.). To deplete splenic MZ B cell and B1 cell precursors, biotinylated antibodies specific for CD9 was added to the above cocktail[31,32]. The unbound cells (typically greater than 90% B220+) were washed and placed into culture at cell densities ranging between 0.3 to 0.5x10^6 cells/ml, depending on the experiment. RPMI 1640 or

IMDM media (Sigma) supplemented with FCS (10% v/v; Genclone), Hepes (10mM; Sigma), Non-essential Amino Acids (1X; Sigma), Glutamax (1X; Invitrogen), Sodium Pyruvate (1X; Sigma), β-ME (55μM; Invitrogen), Penicillin/Streptomycin (1X; Sigma) was used for B cell stimulation. Stimulation involved adding LPS at 10μg/mL (Salmonella enterica serotype typhimurium; Sigma), rhIL-2 at 50U/mL (NCI); and rmIL-5 at 1.5ng/mL (Peprotech). To induce CSR, rmIL-4 was added at 5ng/mL (Peprotech) to LPS cultures. To inhibit PB differentiation, αIgM F(ab')2 was added at 5μg/mL (Southern Biotechnology) to LPS cultures. When cell division was measured, Cell Trace Far Red at 1μM (CTFR; Molecular Probes) was used to label enriched B cells in the presence of PBS for 20min at 37C. Labeling was quenched with growth medium and washed three times before stimulation. Isolated B cells were washed with PBS, loaded with 1μM CTFR (Molecular Probes) prior to culturing. When measuring translation efficiencies, cells were pulsed with the puromycin-containing alkyne, O-Propargyl-puromycin (OPP; Click Chemistry Tools), at 20μM in a humidified CO2 incubator at 37C for 30min prior to processing.

T-independent type 1 challenge

Splenic B cells were isolated from μR x Prdm1:YFP mice (CD45.2) and 1 or 5 million B220+ B cells (experiment 1 or 2, respectively) were injected intravenously into congenic B6.SJL-Ptprca Pepcb/BoyJ (CD45.1) mice. After one day 17ug of LPS (Enzo Life Sciences) was injected intravenously. Three days later the response was quantified by flow cytometry.

ELISA & ELISpot

Secreted IgM was analyzed from supernatants obtained from sorted cells that had been pelleted and resuspended into fresh B cell medium at ~2.25x105/mL for 5 hours in a humidified 37C CO2 incubator. The supernatants were analyzed in duplicate by sandwich ELISA by titration on 96 well

plates in parallel with a purified IgM standard (Sigma). IgM was then detected using an alkaline phosphatase coupled anti-IgM and developed with NPP substrate (Sigma). For ELISpot, 100 cells from populations of interest were sorted into individual wells of a MAHAS4510 filter plate (Millipore) in triplicate containing 0.2mL B cell medium and then incubated for 5 hours in a humidified 37C CO2 incubator. After washing, spots were detected using the same sandwich approach as ELISA; however, the BCIP/NBT substrate (Sigma) was used in place for NPP. The spots were counted using CTL Analyzer and ImmuoSpot Software (Cellular Technology, Ltd.). All ELISA and ELISpot antibodies were purchased from Jackson Immunoresearch.

Flow cytometry

Cells were washed in staining buffer, PBS containing BSA (0.5%, w/v) and sodium azide (0.05%, w/v) and blocked with anti-FcR (clone 2.4G2) hybridoma supernatant. Reporter expression of mAmetrine (excitation/emission of 406/526λ) and mKusabira Orange 2 (excitation/emission of 551/565λ) was visualized following excitation by the violet (405λ) and yellow/green laser (532λ) lasers, respectively. Cells were stained with biotin or fluorochrome coupled antibodies in staining buffer using standard procedures and measured on Symphony SORP cytometer (BD Biosciences). Single color samples were used for pre-acquisition compensation. When performing pre-acquisition compensation of stimulated µR x Prdm1:YFP triple reporter mice, stimulated cells from non-reporter as well as µR-only or Prdm1:YFP-only cells were used. The mA and mKO2 from µR mice was not compensated from each other. FlowJo software (Tree Star, Inc.) was used for flow cytometric and cell division analysis.

When using unfixed cells, dead cells were excluded from analysis using DAPI (Invitrogen). For intracellular detection, cells were pre-stained with Live/Dead Fixable Blue (UV excitable) Stain (Molecular Probes) prior to fixation using 2% (w/v) paraformaldehyde (Electron Microscopy

Sciences) for 60 minutes and then permeabilized and stained using 1X Perm Buffer (eBioscience). This was used in the context of Pax5, IRF4, activated Caspase3, and OPP detection.

Live cells were sorted for ELISpot, ELISA, RNA-seq, and progenitor experiments on an Aria SORP cytometer (BD Biosciences). Dead cells were excluded using DAPI. Single color controls as well as individual reporter mice were used to set up and compensate instrument PMTs. Except for ELISpot experiments, cells were sorted into collection tubes containing an excess of B cell medium. ELISpot experiments involved sorting 100 cells into individual wells of a 96 well filter plate that contained 0.2mL B cell medium. Sorting for ELISA involved 25,000 cells of each population, RNA-seq involved 250,000 cells of each population. For the progenitor experiments, 50,000 cells were sorted; a fraction was immediately rerun on the ARIA prior to reculture. After 23hours, re-cultured cells were also analyzed on the ARIA using the same settings.

Specific Analyses:

- Flow cytometry gating of B cell development: B cell progenitors are B220+CD19+, Pro-B cells are B220+CD19+CD43+IgM-, Large Pre-B cells are B220+CD19+CD43-IgM-FSChi, Small Pre-B are B220+CD19+CD43-FSClo, Immature B are B220+CD19+CD43-IgM+, Circulating Mature B are B220hiCD19+CD43-IgM+.
- Flow cytometry gating of Peripheral B cell development: Germinal Center B cells are B220+IgDloFashiCD38lo. Plasma cells are CD19hi/loF4/80-IgDloSca1+Synd1+.
- When quantifying ER biomass in live cells, ER-Tracker™ Red (BODIPY™ TR Glibenclamide; Molecular Probes) was added to cells (0.5µM) that had been washed into PBS (Ca++Mg++ free) multiple times and incubated at 37C for 20min in 5% CO2 incubator prior to washing in staining buffer and analysis on the cytometer. Dead cells were excluded using DAPI (Molecular Probes).

- When measuring translation efficiencies, OPP (20μM, 20min, 37C in 5% CO2 incubator) pulsed cells were washed, labeled with Live/Dead Fixable Blue (UV excitable) Stain (Molecular Probes), fixed using 2% (w/v) paraformaldehyde (Electron Microscopy Sciences) for 60 minutes, and permeabilized with 1X Perm Buffer (eBioscience). The Click reaction, to covalently react the fluorescent AF647 azide to the alkyne incorporated into nascent protein was performed using a kit and protocols from Click Chemistry Tools.
- When analyzing B cells following T-independent type 1 responses, cells were gated on a given CD45 allotype to distinguish μR from host and then on B220hi/medium.

RNA-seq

Total RNA was extracted from cell pellets using Trizol (Invitrogen, 15596018). Complementary DNA (cDNA) libraries for Illumina sequencing were generated using the TruSeq Stranded mRNA Library Prep kit (Illumina, cat: 20020595), following the manufacturer's instructions. The libraries were subsequently sequenced on a NovaSeq 6000 platform using a paired-end S4 flow cell. Adapters and low-quality reads were removed from the raw fastq files using Cutadapt[43]. The paired-end reads were aligned to the mouse genome (mm9) using STAR[44], and differential expression analysis was performed using edgeR[45]. RNA-seq data was computed using 2 or 3 replicates per group. This data has been deposited into NCBI GEO as accession GSE242335.

Quantification and statistical analysis

Software used include Excel for statistical analysis, Flowjo for flow cytometry analysis, and R for RNA-seq analysis. Results from unpaired t-tests are described in the Results and Figure Legends. Significance is indicated by asterisks and is defined as $p<0.05$. A biological replicate indicates an animals used.

References

1. Boothby, M. R., Hodges, E. & Thomas, J. W. Molecular regulation of peripheral B cells and their progeny in immunity. *Genes Dev.* **33**, 26–48 (2019). https://doi.org/10.1101/gad.320192.118
2. Cyster, J. G. & Allen, C. D. C. B Cell Responses: Cell Interaction Dynamics and Decisions. *Cell* **177**, 524–540 (2019). https://doi.org/10.1016/j.cell.2019.03.016
3. Alt, F. W. *et al.* Synthesis of secreted and membrane-bound immunoglobulin mu heavy chains is directed by mRNAs that differ at their 3' ends. *Cell* **20**, 293–301 (1980). https://doi.org/10.1016/0092-8674(80)90615-7
4. Early, P. *et al.* Two mRNAs can be produced from a single immunoglobulin mu gene by alternative RNA processing pathways. *Cell* **20**, 313–319 (1980). https://doi.org/10.1016/0092-8674(80)90617-0
5. Rogers, J. *et al.* Two mRNAs with different 3' ends encode membrane-bound and secreted forms of immunoglobulin mu chain. *Cell* **20**, 303–312 (1980). https://doi.org/10.1016/0092-8674(80)90616-9
6. Potter, M. Immunoglobulin-producing tumors and myeloma proteins of mice. *Physiol Rev* **52**, 631–719 (1972). https://doi.org/10.1152/physrev.1972.52.3.631
7. Cook, S. L., Franke, M. C., Sievert, E. P. & Sciammas, R. A Synchronous IRF4-Dependent Gene Regulatory Network in B and Helper T Cells Orchestrating the Antibody Response. *Trends Immunol* **41**, 614–628 (2020). https://doi.org/10.1038/ni.1900
8. Goodnow, C. C., Vinuesa, C. G., Randall, K. L., Mackay, F. & Brink, R. Control systems and decision making for antibody production. *Nat Immunol* **11**, 681–688 (2010). https://doi.org/10.1038/ni.1900
9. Low, M. S. Y. *et al.* IRF4 Activity Is Required in Established Plasma Cells to Regulate Gene Transcription and Mitochondrial Homeostasis. *Cell Rep* **29**, 2634-2645.e5 (2019). https://doi.org/10.1016/j.celrep.2019.10.097
10. Tellier, J. *et al.* Blimp-1 controls plasma cell function through the regulation of immunoglobulin secretion and the unfolded protein response. *Nat Immunol* **17**, 323–330 (2016). https://doi.org/10.1038/ni.3348

11. Nutt, S. L., Hodgkin, P. D., Tarlinton, D. M. & Corcoran, L. M. The generation of antibody-secreting plasma cells. *Nat Rev Immunol* **15**, 160–171 (2015). https://doi.org/10.1038/nri3795
12. Ricci, D., Gidalevitz, T. & Argon, Y. The special unfolded protein response in plasma cells. *Immunol Rev* **303**, 35–51 (2021). https://doi.org/10.1111/imr.13012
13. Kallies, A. *et al.* Initiation of plasma-cell differentiation is independent of the transcription factor Blimp-1. *Immunity* **26**, 555–566 (2007). https://doi.org/10.1084/jem.20161122
14. Savage, H. P. *et al.* Blimp-1-dependent and -independent natural antibody production by B-1 and B-1-derived plasma cells. *J Exp Med* **214**, 2777–2794 (2017). https://doi.org/10.1084/jem.20161122
15. Alt, F. W., Rosenberg, N., Enea, V., Siden, E. & Baltimore, D. Multiple immunoglobulin heavy-chain gene transcripts in Abelson murine leukemia virus-transformed lymphoid cell lines. *Mol Cell Biol* **2**, 386–400 (1982). https://doi.org/10.1128/mcb.2.4.386-400.1982
16. Bayles, I. & Milcarek, C. Plasma cell formation, secretion, and persistence: the short and the long of it. *Crit Rev Immunol* **34**, 481–499 (2014). https://doi.org/10.1615/critrevimmunol.2014012168
17. Matis, S. A., Martincic, K. & Milcarek, C. B-lineage regulated polyadenylation occurs on weak poly(A) sites regardless of sequence composition at the cleavage and downstream regions. *Nucleic Acids Res* **24**, 4684–4692 (1996). https://doi.org/10.1093/nar/24.23.4684
18. Peterson, M. L., Gimmi, E. R. & Perry, R. P. The developmentally regulated shift from membrane to secreted mu mRNA production is accompanied by an increase in cleavage-polyadenylation efficiency but no measurable change in splicing efficiency. *Mol Cell Biol* **11**, 2324–2327 (1991). https://doi.org/10.1128/mcb.11.4.2324
19. Martincic, K., Alkan, S. A., Cheatle, A., Borghesi, L. & Milcarek, C. Transcription elongation factor ELL2 directs immunoglobulin secretion in plasma cells by stimulating altered RNA processing. *Nat Immunol* **10**, 1102–1109 (2009). https://doi.org/10.1038/ni.178620.

Sciammas, R. *et al.* Graded expression of interferon regulatory factor-4 coordinates isotype switching with plasma cell differentiation. *Immunity* **25**, 225–236 (2006). https://doi.org/10.1016/j.immuni.2006.07.009
21. Sciammas, R. & Davis, M. M. Modular nature of Blimp-1 in the regulation of gene expression during B cell maturation. *J Immunol* **172**, 5427–5440 (2004). https://doi.org/10.4049/jimmunol.172.9.5427

22. Pettersson, S., Cook, G. P., Brüggemann, M., Williams, G. T. & Neuberger, M. S. A second B cell-specific enhancer 3' of the immunoglobulin heavy-chain locus. *Nature* **344**, 165–168 (1990). https://doi.org/10.1038/344165a0
23. Ji, Z. *et al.* Transcriptional activity regulates alternative cleavage and polyadenylation. *Mol Syst Biol* **7**, 534 (2011). https://doi.org/10.1038/msb.2011.69
24. Cheng, R. Y.-H. *et al.* SEC-seq: association of molecular signatures with antibody secretion in thousands of single human plasma cells. *Nat Commun* **14**, 3567 (2023). https://doi.org/10.1038/s41467-023-39367-8
25. Eyer, K. *et al.* Single-cell deep phenotyping of IgG-secreting cells for high-resolution immune monitoring. *Nat Biotechnol* **35**, 977–982 (2017). https://doi.org/10.1038/nbt.3964
26. Jung, D., Giallourakis, C., Mostoslavsky, R. & Alt, F. W. Mechanism and control of V(D)J recombination at the immunoglobulin heavy chain locus. *Annu Rev Immunol* **24**, 541–570 (2006). https://doi.org/10.1146/annurev.immunol.23.021704.115830
27. Kemp, D. J., Wilson, A., Harris, A. W. & Shortman, K. The immunoglobulin mu constant region gene is expressed in mouse thymocytes. *Nature* **286**, 168–170 (1980). https://doi.org/10.1038/286168a0
28. Bachl, J., Turck, C. W. & Wabl, M. Translatable immunoglobulin germ-line transcript. *Eur J Immunol* **26**, 870–874 (1996). https://doi.org/10.1002/eji.1830260422
29. Roco, J. A. *et al.* Class-Switch Recombination Occurs Infrequently in Germinal Centers. *Immunity* **51**, 337-350.e7 (2019). https://doi.org/10.1016/j.immuni.2019.07.001
30. Fooksman, D. R. *et al.* Development and migration of plasma cells in the mouse lymph node. *Immunity* **33**, 118–127 (2010). https://doi.org/10.1016/j.immuni.2010.06.015
31. Ha, S. *et al.* Regulation of B1 cell migration by signals through Toll-like receptors. *J Exp Med* **203**, 2541–2550 (2006). https://doi.org/10.1084/jem.20061041
32. Lopes-Carvalho, T. & Kearney, J. F. Development and selection of marginal zone B cells. *Immunological Reviews* **197**, 192–205 (2004). https://doi.org/10.1111/j.0105-2896.2004.0112.x
33. Chen-Bettecken, U., Wecker, E. & Schimpl, A. IgM RNA switch from membrane to secretory form is prevented by adding antireceptor antibody to bacterial lipopolysaccharide-stimulated murine primary B-cell cultures. *Proc Natl Acad Sci U S A* **82**, 7384–7388 (1985). https://doi.org/10.1073/pnas.82.21.7384

34. Schliephake, D. E. & Schimpl, A. Blimp-1 overcomes the block in IgM secretion in lipopolysaccharide/anti-mu F(ab')2-co-stimulated B lymphocytes. *Eur J Immunol* **26**, 268–271 (1996). https://doi.org/10.1002/eji.1830260142
35. Pinaud, E. *et al.* The IgH locus 3' regulatory region: pulling the strings from behind. *Adv Immunol* **110**, 27–70 (2011). https://doi.org/10.1016/B978-0-12-387663-8.00002-8
36. Minnich, M. *et al.* Multifunctional role of the transcription factor Blimp-1 in coordinating plasma cell differentiation. *Nat Immunol* **17**, 331–343 (2016). https://doi.org/10.1038/ni.3349
37. Lam, J. H. & Baumgarth, N. The Multifaceted B Cell Response to Influenza Virus. *J Immunol* **202**, 351–359 (2019). https://doi.org/10.4049/jimmunol.1801208
38. Seidl, K. J. *et al.* Position-dependent inhibition of class-switch recombination by PGK-neor cassettes inserted into the immunoglobulin heavy chain constant region locus. *Proc Natl Acad Sci U S A* **96**, 3000–3005 (1999). https://doi.org/10.1073/pnas.96.6.3000
39. Köntgen, F., Süss, G., Stewart, C., Steinmetz, M. & Bluethmann, H. Targeted disruption of the MHC class II Aa gene in C57BL/6 mice. *Int Immunol* **5**, 957–964 (1993). https://doi.org/10.1093/intimm/5.8.957
40. Mittrücker, H. W. *et al.* Requirement for the transcription factor LSIRF/IRF4 for mature B and T lymphocyte function. *Science* **275**, 540–543 (1997). https://doi.org/10.1126/science.275.5299.540
41. Rickert, R. C., Rajewsky, K. & Roes, J. Impairment of T-cell-dependent B-cell responses and B-1 cell development in CD19-deficient mice. *Nature* **376**, 352–355 (1995). https://doi.org/10.1038/376352a0
42. Shapiro-Shelef, M. *et al.* Blimp-1 is required for the formation of immunoglobulin secreting plasma cells and pre-plasma memory B cells. *Immunity* **19**, 607–620 (2003). https://doi.org/10.1016/s1074-7613(03)00267-x
43. Martin, M. Cutadapt removes adapter sequences from high-throughput sequencing reads. *EMBnet j.* **17**, 10 (2011). https://doi.org/10.14806/ej.17.1.200
44. Dobin, A. *et al.* STAR: ultrafast universal RNA-seq aligner. *Bioinformatics* **29**, 15–21 (2013). https://doi.org/10.1093/bioinformatics/bts635
45. Robinson, M. D., McCarthy, D. J. & Smyth, G. K. edgeR: a Bioconductor package for differential expression analysis of digital gene expression data. *Bioinformatics* **26**, 139–140 (2010). https://doi.org/10.1093/bioinformatics/btp616

Figure 4

Signaling or genetic inhibition of PB differentiation prevents graded μS PAS usage

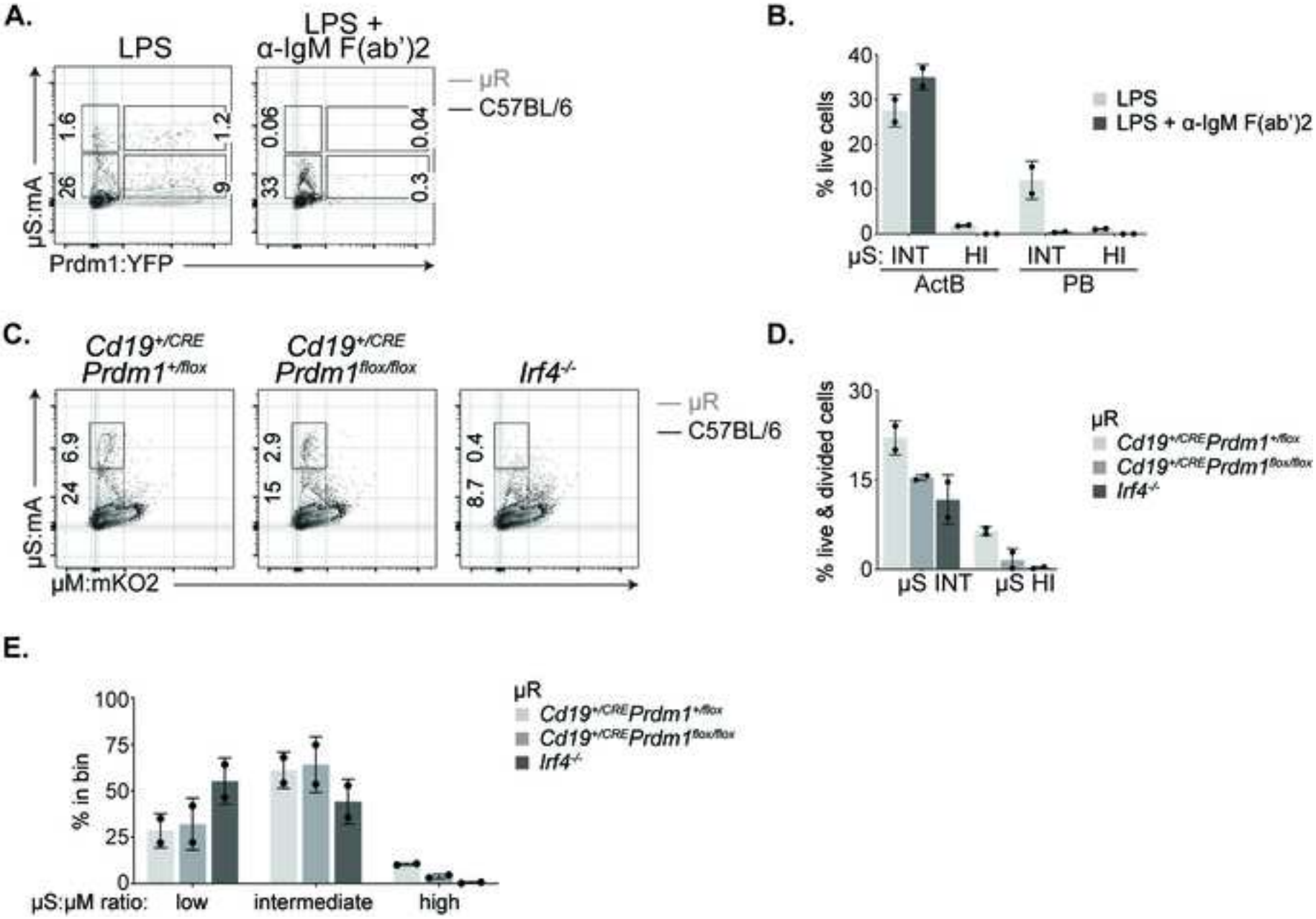

Figure 5

Transcriptional differences associated with graded μS PAS usage and Prdm1:YFP expression

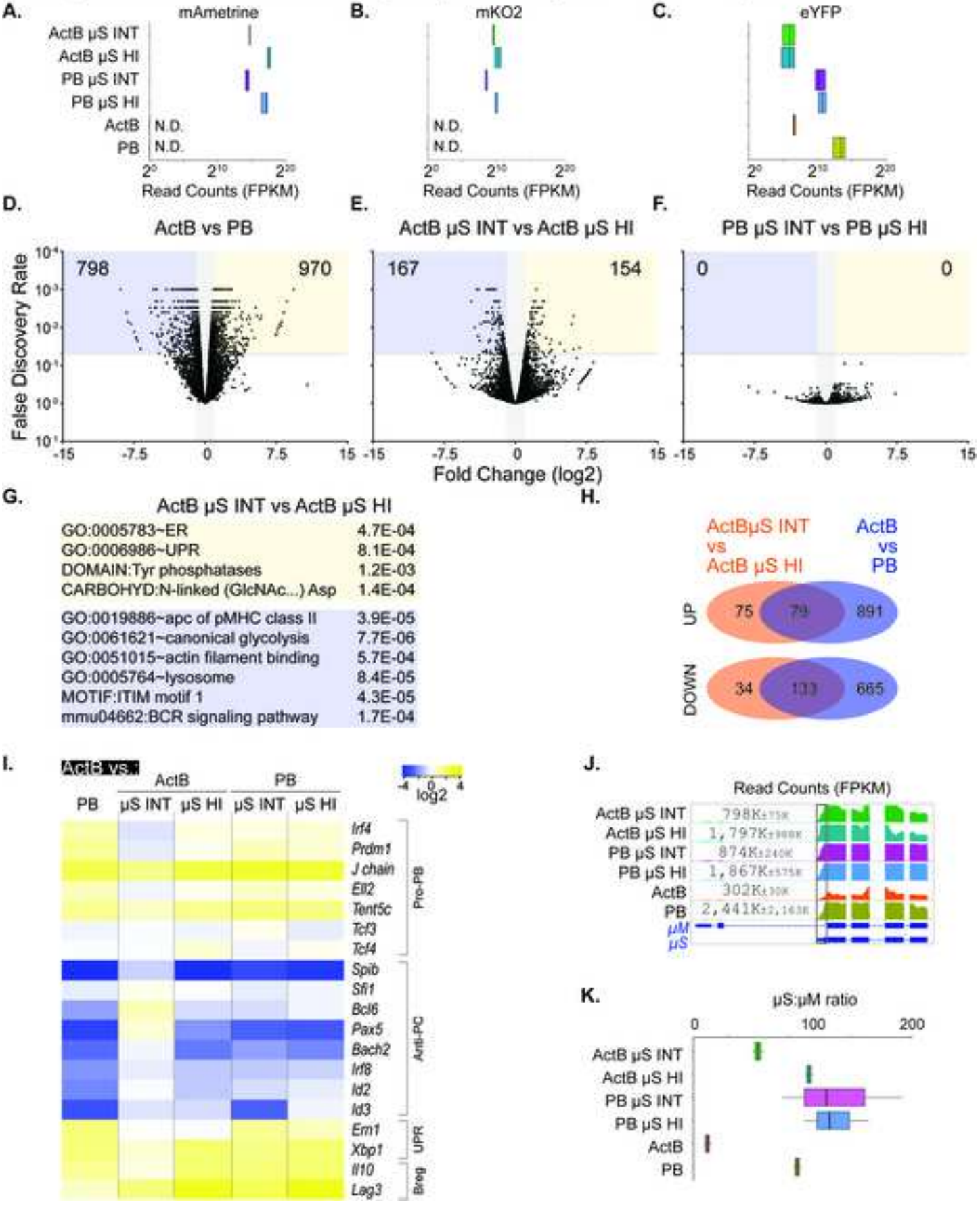

Figure 6
Progenitor fate trajectories of graded μS cells that are Prdm1:YFP expressing or not

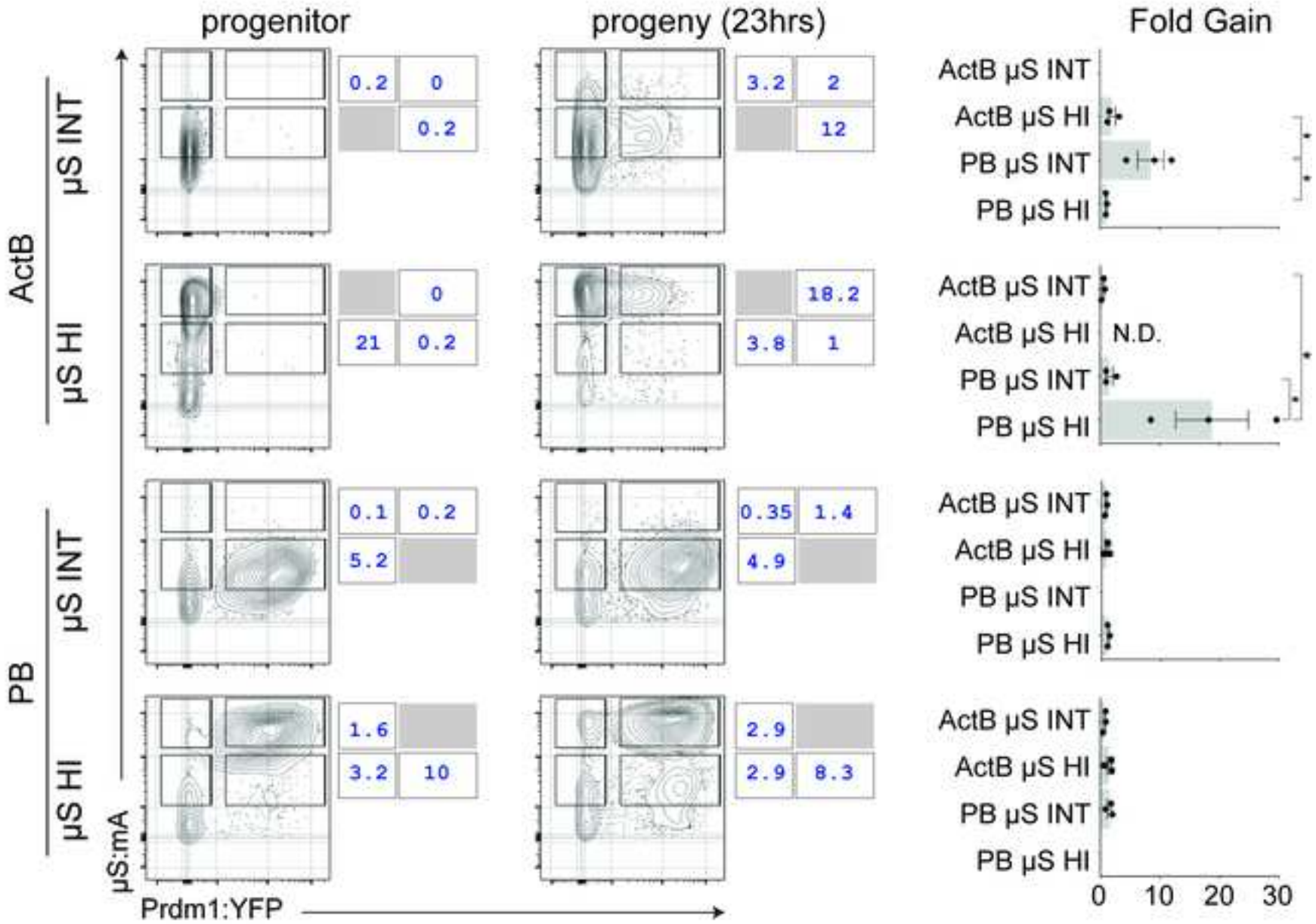

Figure 7
Expression of cell biological, B lineage, PB features or ER associated genes among graded μS populations that express Prdm1:YFP or not

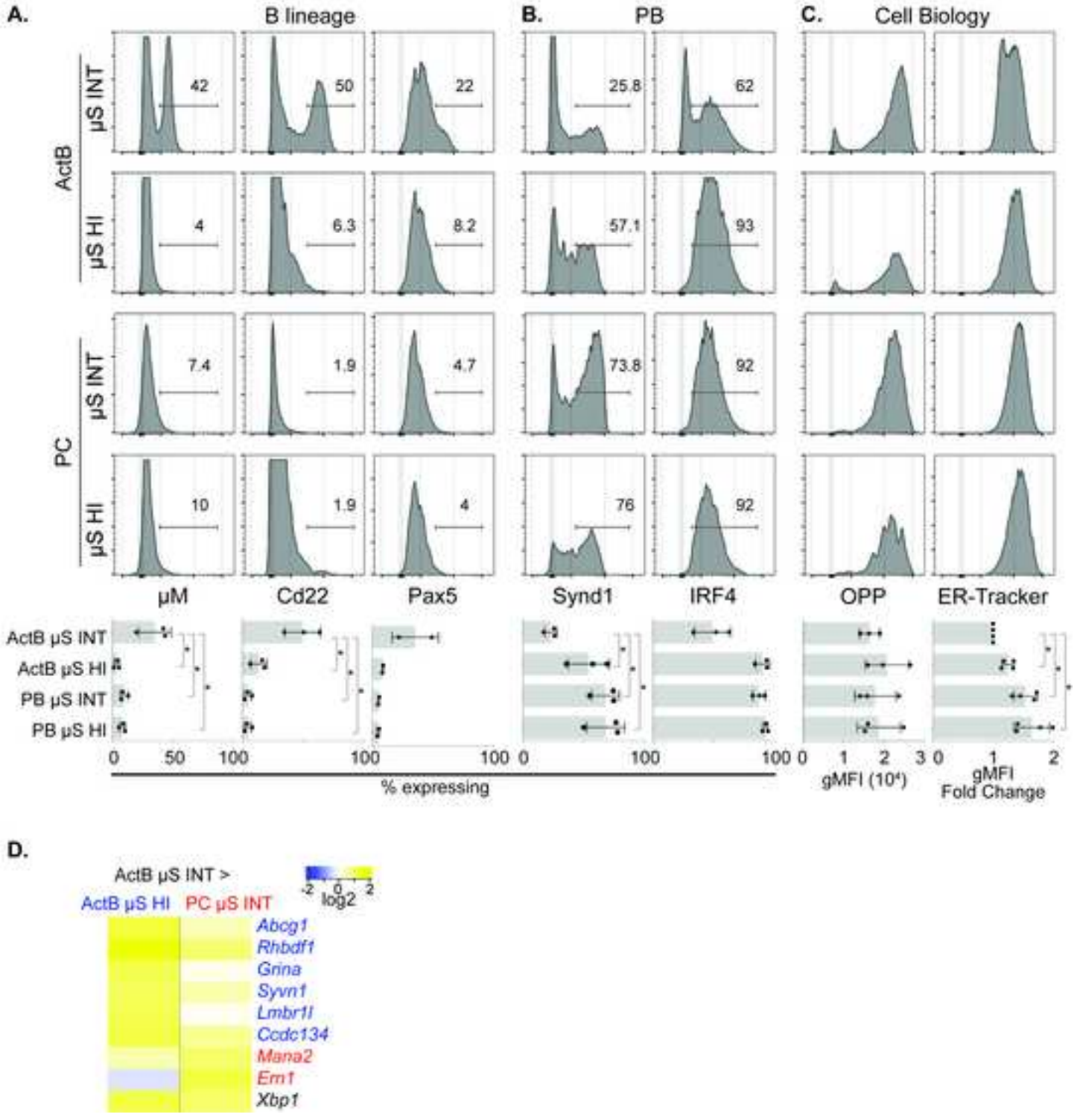

Figure 1
Generation of μR mice that encode dual fluorescent reporters to enumerate B cells undergoing alternative μM and μS PAS usage

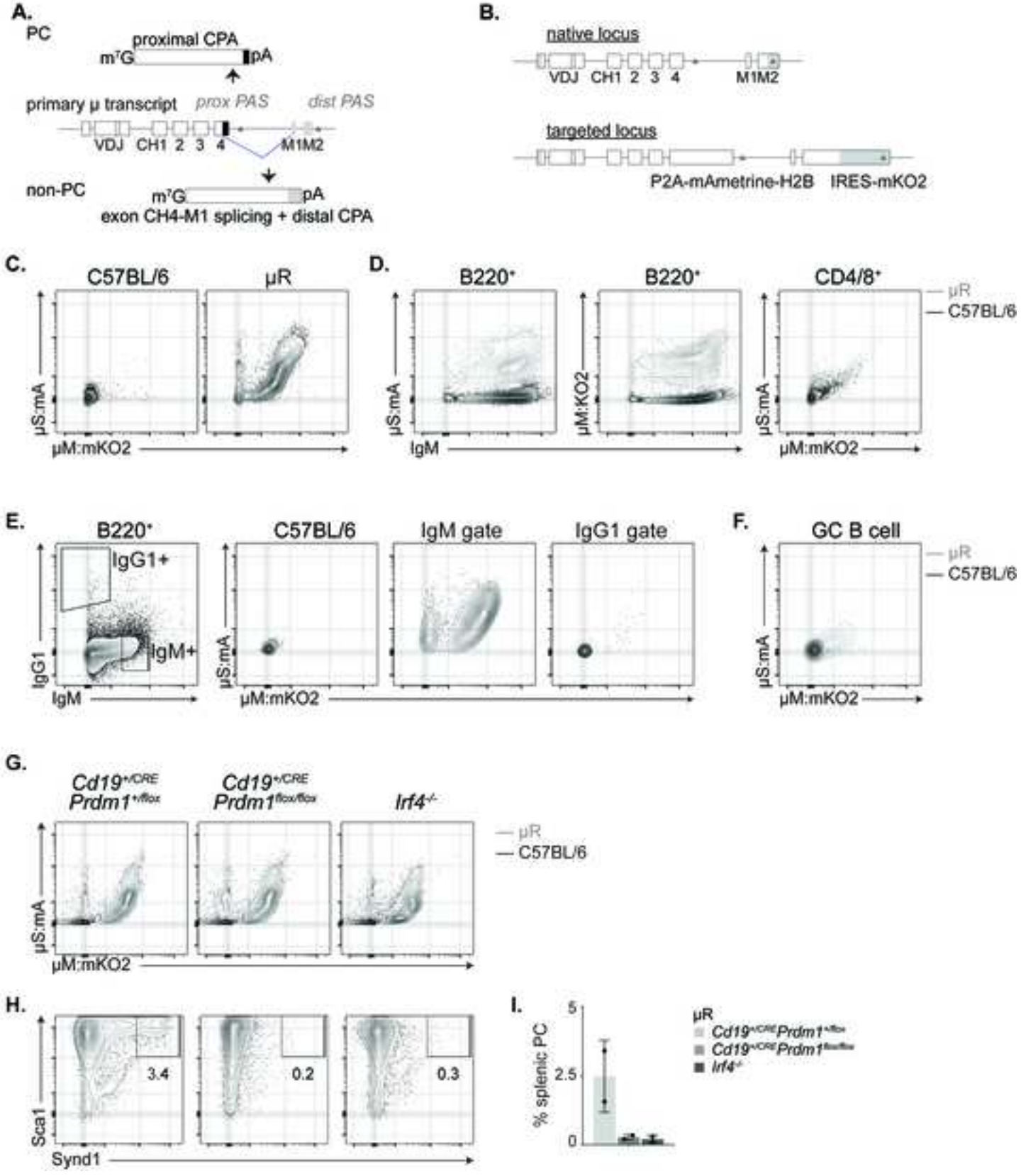

Figure 2
B cell stimulation results in de novo μR reporter expression that display graded μS PAS usage

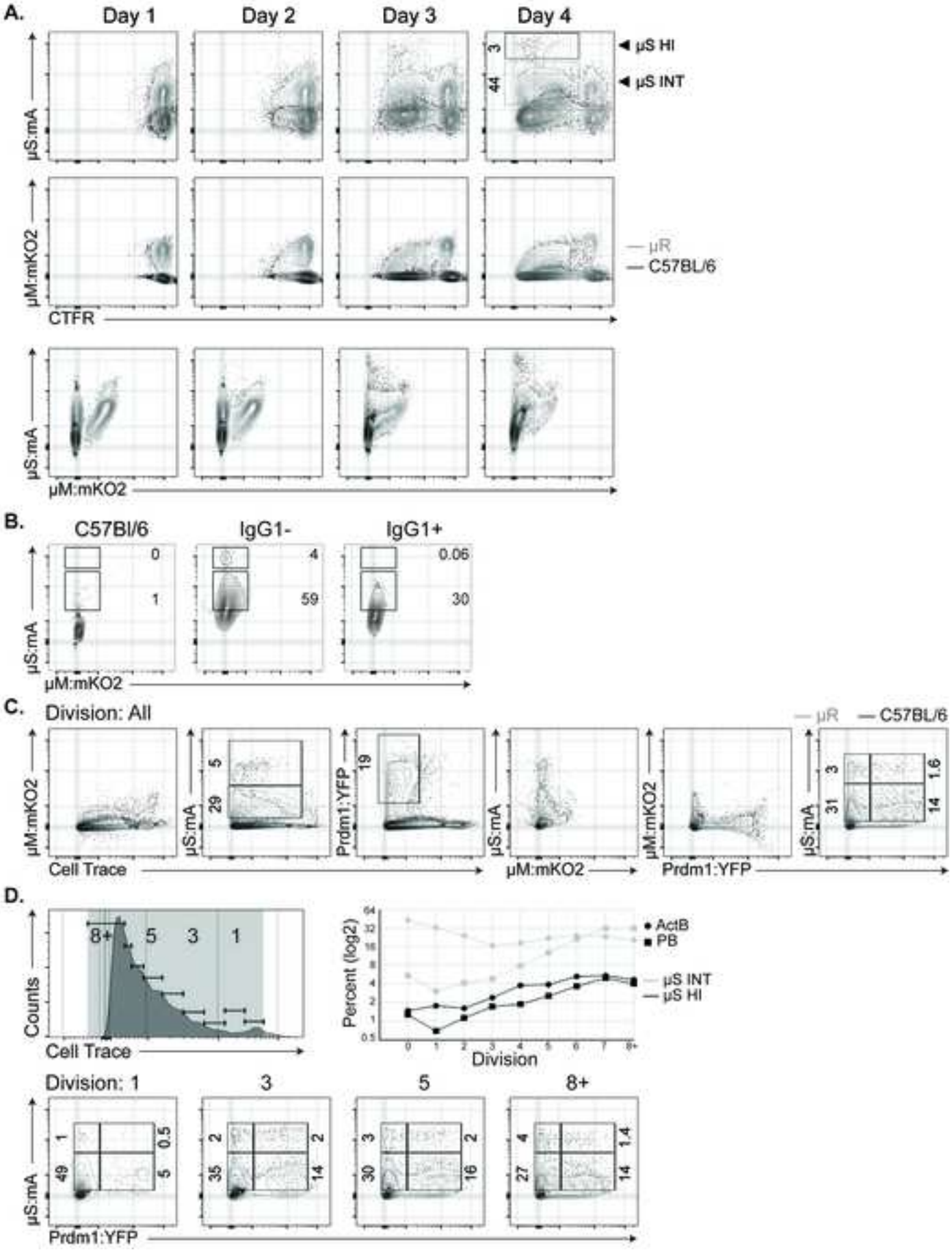

Figure 3
μS:mA expression marks secreting cells

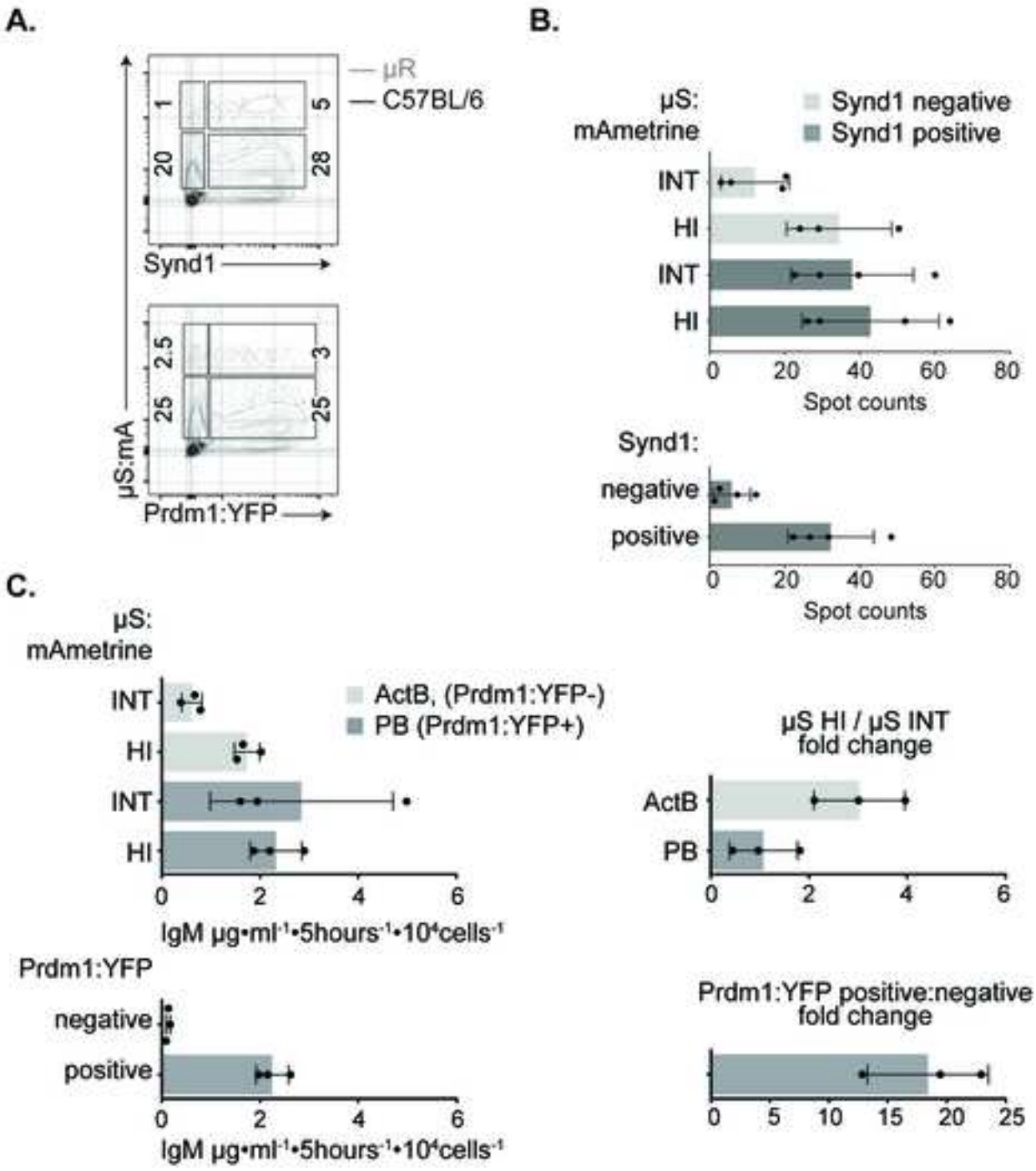

Supplemental figure titles and legends

Supplemental Figure 1. Engineering and validation of μReporter mice. Related to Figure 1.

A. IgH6 (μ) locus configuration, top. IgH6 locus after homologous recombination, middle. Recombined IgH6 locus after Flpe-mediated removal of frt-flanked neomycin selection cassette.

B. PCR genotyping of wildtype, heterozygous, and homozygous IgH6 targeted mice.

Supplemental Figure 2. μS PAS usage in developmental B cell subsets and ex vivo Plasma cells. Related to Figure 1.

A. Enumeration of developmental B cell subsets between control C57Bl/6 and μR heterozygous mice. Gating strategy is described in Methods section. Each point represents measurements from different mice.

B. Patterns of μR reporter expression during development and in peripheral B cell subsets. Gating strategy is described in Methods section.

C. Patterns of uR reporter expression in bone marrow Plasma cells gated as CD19hi/loCD4-F4/80-Sca1+Synd1+.

Supplemental Figure 3. ActB cells that display μS INT PAS usage rates do not express switched isotypes, ActB cells that display μS HI PAS usage rates not exclusively derived from B1 cells, and ActB or PB cells that display μS INT or μS HI PAS usage rates arise after T-independent type 1 responses in vivo. Related to Figure 2.

A. Analysis of μS:mA expression in relation to switched isotype expression following stimulation of enriched splenic B cells with LPS and IL2/IL5 cytokines at Day 4. Cells were stained with the indicated Ig isotypes and DAPI-excluded cells were analyzed by flow cytometry. We note that under this stimulation conditions, there is only induced class switch recombination to IgG3 and that other isotypes detected likely occurred in vivo and responded to LPS in vitro. Representative of 3 independent biological replicates.

B. Analysis of LPS-induced μS:mA and Prdm1:YFP expression after depletion of Marginal Zone and B1 B cells. Splenic B cells from μR x Prdm1:YFP mice were immunomagnetically enriched using a cocktail of lineage specific biotinylated antibodies that included one specific for CD9 that is highly expressed by Marginal Zone, B1, and Plasma cells. Enriched cells were stimulated with LPS and IL2/IL5 cytokines for 4 days and then DAPI-excluded cells were analyzed by flow cytometry. Representative of 2 independent biological replicates.

C. Analysis of μS:mA and Prdm1:YFP expression in vivo following T-Independent type 1 challenge. CD45.2-expressing μR x Prdm1 cells were adoptively transferred into CD45.1 expressing congenic host mice and then challenged with LPS. Three days later, splenic cells were stained with antibodies specific to CD45.2, CD45.1, and B220. Donor μR x Prdm1 cells were gates as CD45.2+CD45.1-B220hi/med. Overlayed are CD45.1+CD45.2-B220hi/med non-fluorescent host B cells. Shown in the 4 plots on the left are the μR and Prdm1:YFP expression patterns from observed in 4 individual recipient mice; the last plot on the right is concatenation of the four individual results. A second independent biological replicate using 2 host mice resulted in comparable results.

Supplement Figure 1
Engineering and validation of µReporter mice

A.

IgH6_ENSMUSG00000076617

IgH6 knock-in_ENSMUSG00000076617

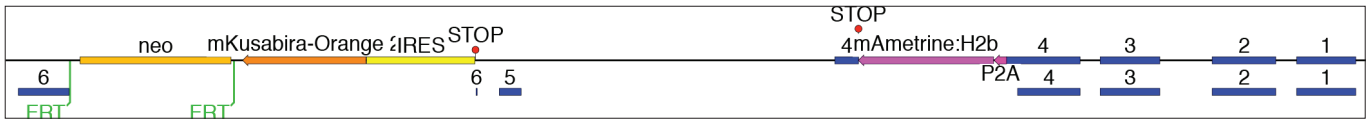

µReporter

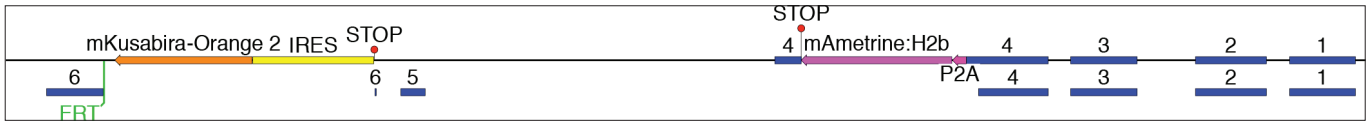

B.

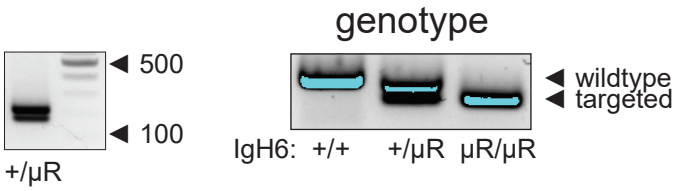

Supplement Figure 2
μS PAS usage in developmental B cell subsets and ex vivo Plasma cells

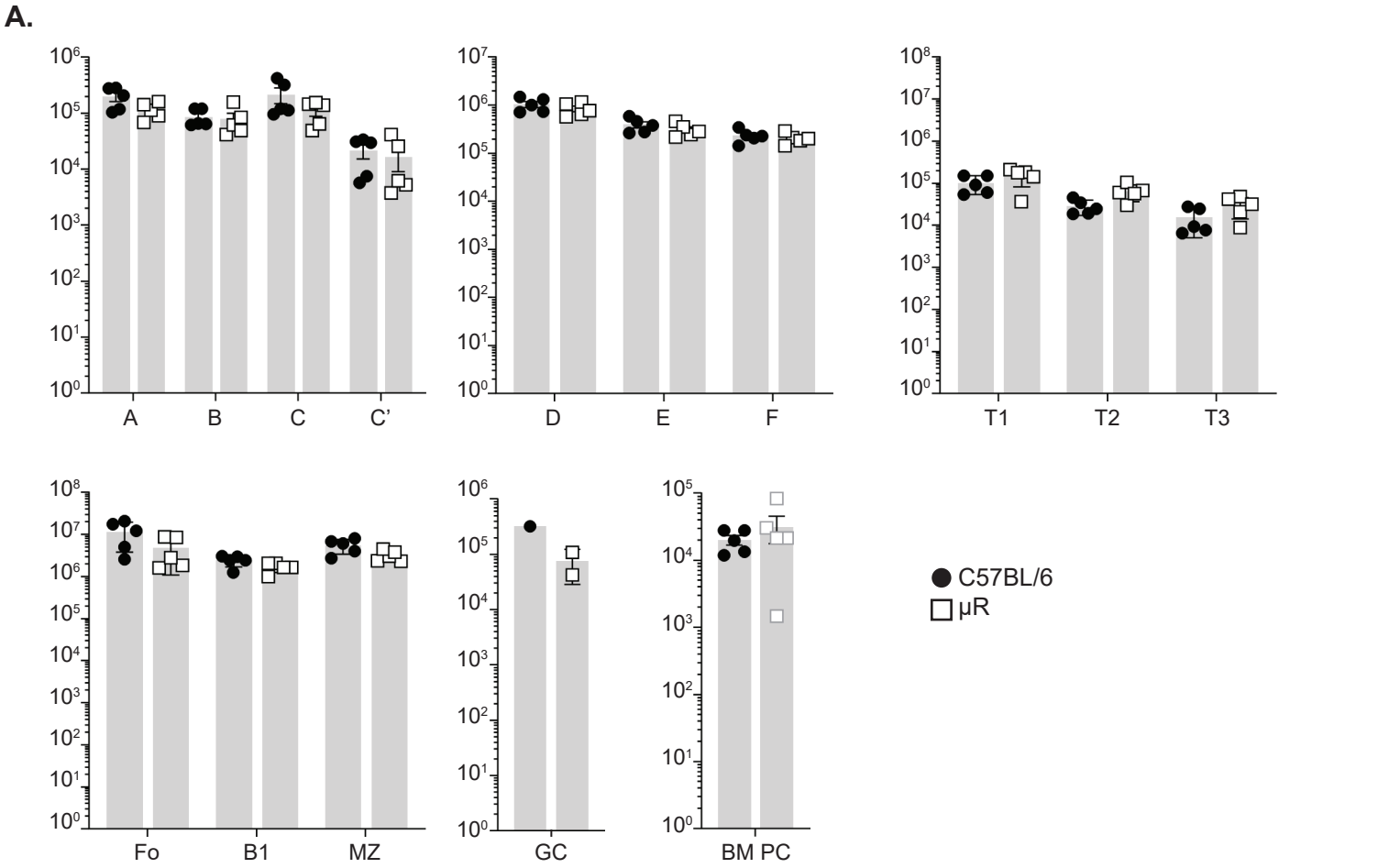

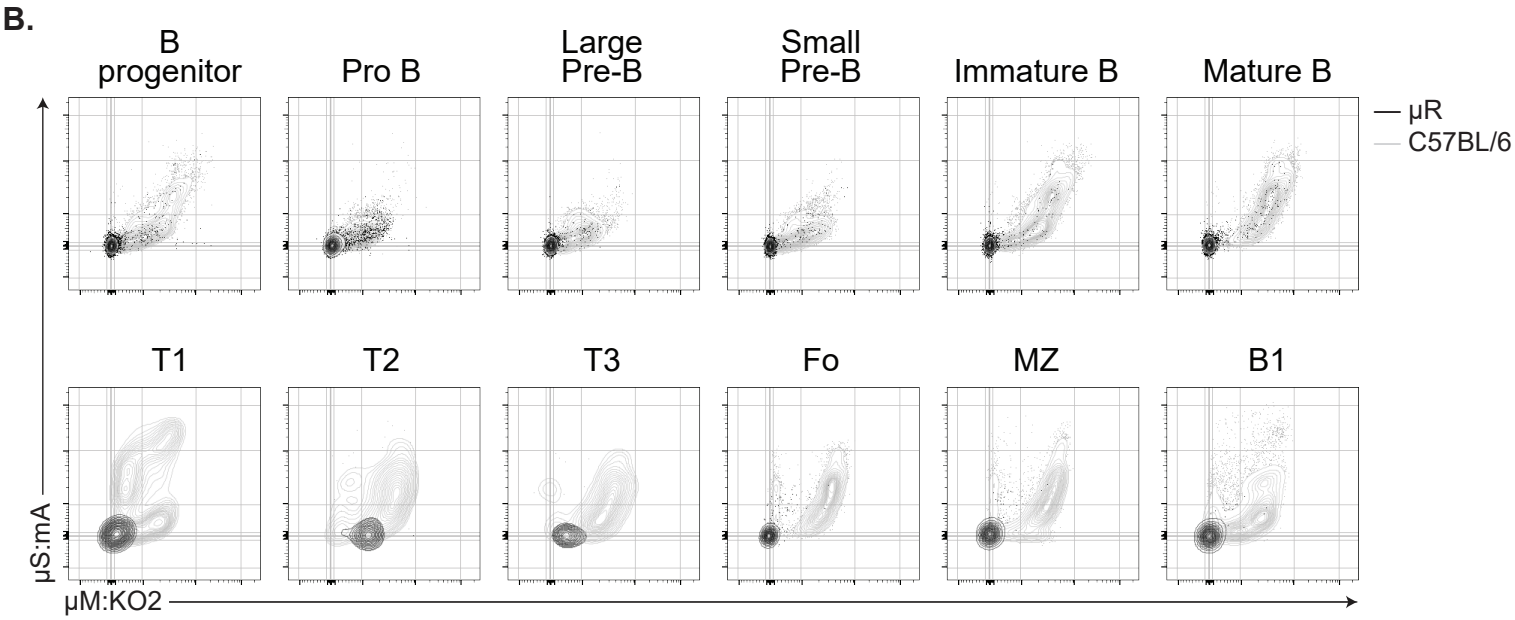

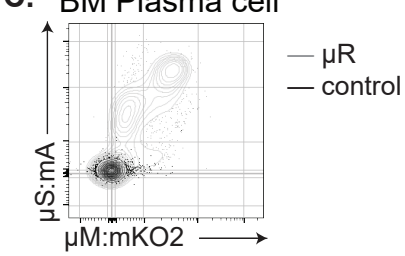

Supplement Figure 3
ActB cells that display μS INT PAS usage rates do not express switched isotypes, ActB cells that display μS HI PAS usage rates not exclusively derived from B1 cells, and ActB or PB cells that display μS INT or μS HI PAS usage rates arise after T-independent type 1 responses in vivo